The Design of the New HPA Personal Thermoluminescence Dosemeter

J S Eakins

Centre for Radiation, Chemical and Environmental Hazards
Radiation Protection Division
Chilton, Didcot, Oxfordshire OX11 0RQ

Approval: October 2010
Publication: October 2010
£21.00
ISBN 978-0-85951- 677-8

EXECUTIVE SUMMARY

This document describes the optimization and evaluation of the new HPA thermoluminescence dosemeter (TLD), designed for use in mixed photon / electron fields with energies in the range from ~10 keV to ~10^4 keV. The Monte Carlo simulation package MCNP4c2 was used primarily, with additional measurements performed where possible. The basic configuration modelled consisted of a Harshaw TLD-700H 'card' encased inside a plastic holder, located on a water-filled ISO slab phantom. The purpose of the holder is to not only protect the card, but also to incorporate a suitable attenuating filter that yields an accurate $H_p(10)$ dose response characteristic in the lithium fluoride detector.

In an effort to emulate the properties of tissue, and hence provide a good $H_p(10)$ response, a number of different filter materials and geometries were investigated. An 18 mm diameter, 4.3 mm thick disk of PTFE covered by 2 mm thick polypropylene finally emerged as the best filter candidate, giving the most acceptable relative response found in this study against the desired criteria. Both the $H_p(10)$ and $H_p(0.07)$ responses of a device incorporating such a filter were investigated, using the full ISO Narrow-Series energy spectra data and ^{137}Cs, ^{60}Co, $^{12}C(p,p'\gamma)^{12}C$ and $^{19}F(p,\alpha\gamma)^{16}O$ sources at incident angles of 0°, ±30° and ±60°. Rotational (-80° to +80°), average lateral (-120° to -60° and 60° to +120°) and vertical (30° and 60° from above) relative response performances were also determined, as well as the $H^*(10)$ response of the device off-phantom in an isotropic field.

Generally, the design programme progressed using the kerma approximation and photon-only transport in the Monte Carlo simulations. However, calculations involving the more computationally-demanding full electron-photon transport mode of MCNP were also performed, in order to confirm the suitability of the filter of the final design in fields containing electrons.

Comparisons were made with experimental data, where available. The benefits of such a process were twofold: serving to validate the calculated results; and also providing an improved handle on the intrinsic efficiency of the lithium fluoride detector.

As an additional check of the reliability of the MCNP procedure, air kerma to $H_p(10)$ conversion coefficients were also determined and compared against accepted standards. Good agreement is reported.

Finally, since completing the optimization project, the updated Monte Carlo package MCNP5 became available. The impact of using this on calculations of the response of the final design of TLD was investigated. Low energy (< 50 keV) discrepancies of up to ~10 % were demonstrated between MCNP4c2 and MCNP5 results, which can be attributed to the updated photoelectric effect cross section tables that are available with MCNP5.

CONTENTS

1	**Introduction**	**1**
2	**Problem Description**	**1**
	2.1 Design Requirements	**1**
	2.1.1 International Standards	2
	2.1.2 European Recommendations	2
	2.1.3 UK Requirements	3
	2.2 Design Specifications	**3**
	2.3 MCNP Simulation	**5**
3	**Preliminary Work and Remarks**	**7**
	3.1 Filter Alternatives	**8**
	3.2 Source Field	**9**
	3.3 Efficiency Function	**9**
	3.4 PP Thickness Variation	**11**
4	**The PTFE Slab Filter**	**11**
5	**The 3.73 mm PTFE Disk Filter**	**14**
6	**Thicker Disks**	**18**
7	**Rotational Irradiation**	**22**
8	**Lateral Irradiation**	**24**
9	**Vertical Irradiation**	**25**
10	**Electron Filtration**	**26**
	10.1 Attenuation	**26**
	10.2 Fluence-Energy Distribution	**28**
11	**Method Validation: Conversion Coefficients Calculation**	**29**
	11.1 PTB Sources	**30**
	11.2 Monoenergetic Sources	**31**
12	**Experimental Type-Testing**	**32**
13	**MCNP4c2 versus MCNP5**	**32**
14	***H**(10) Response**	**34**
15	**Summary and Conclusions**	**37**
16	**Acknowledgements**	**38**
17	**References**	**39**
APPENDIX A		**41**
	Change Log	
APPENDIX B		**44**
	MCNP Input File for Air Kerma Determination	

APPENDIX C **49**
MCNP Input File for Slab Filter Design

APPENDIX D **53**
MCNP Input File for Final Design

1 INTRODUCTION

In order to monitor the levels of personal dose equivalent to which workers are exposed in environments containing electrons and photons, the HPA Personal Dosimetry Service (PDS) provides passive thermoluminescence dosemeters (TLDs). Recently, however, there was a desire to update the HPA system: the existing system was very old, the readers were becoming increasingly unreliable, and it was becoming harder to obtain spare parts. Additionally, lithium fluoride doped with magnesium, copper and phosphorus had been shown to exhibit better dosimetric properties than the magnesium and titanium material that was used in the NRPB (now HPA) service [Moskovich et al 2006; Hranitzky et al, 2006]. It was hence an opportune time to simultaneously update the hardware associated with the service and move to a thermoluminescent material that could offer better dosimetric properties.

A decision was made to adopt the Harshaw TLD-700H 'card', which has a different size and shape from the NRPB version [Shaw, 1977] that had been in use previously. As a consequence, the holder housing the TLD card needed to be redesigned, partly as a result of requiring different internal dimensions, but partly also in an attempt to better the overall performance of the device. The aim was to develop an improved TLD for personal monitoring that is capable of accurately assessing $H_p(10)$ and $H_p(0.07)$ in electron / photon radiation fields with energies from ~10^4 to ~10^7 eV.

As a way of investigating the effects of various proposed changes to the holder design, the Monte Carlo simulation software MCNP4c2 [Briesmeister, 2000] was used to evaluate the performance of the suggested alternatives. The hope, of course, was that this process would ultimately converge upon an optimum design. The present document reports on that process, and effectively provides a chronological account of the key stages that took place on the way towards the acceptance of the final design. The report thus represents an extensive overview of the entire TLD development project, from the design stages to the assessment of the final device, whilst also serving to expand or summarize discussions provided in work published elsewhere [Eakins *et al* 2007a; Eakins *et al* 2007b; Gilvin *et al* 2007; Eakins 2008; Eakins 2009].

2 PROBLEM DESCRIPTION

2.1 Design Requirements

Even before beginning, the ultimate design of the dosemeter was already reasonably well-constrained within certain parameters, due to a number of external factors. Apart from physical size and shape, such considerations included cost, practicality, aesthetics, ease of manufacture, etc. Moreover, whatever else it may involve, the final holder design necessarily demanded some form of hole to allow for $H_p(0.07)$ detection, some form of viewing window to permit card label identification, and some form of filter to account for $H_p(10)$ response. The latter must be such that it provides filtration equivalent to 10 mm of tissue, but ideally it should not protrude by as much as 10 mm from the

front of the dosemeter, partly to avoid shadowing of the $H_p(0.07)$ element, but also for aesthetic reasons. So, the 'best' design optimizes all of these requirements together, to one extent or another, within an acceptable level of compromise.

The $H_p(10)$ energy and angle dependence of response of the dosemeter is intended for a stated range of use for photon energies from 15 keV to 7 MeV and for: angles of incidence up to 60°; irradiation from the side; and irradiation in isotropic fields. The energy limits correspond to the minimum and maximum distributions typically available as ISO reference fields [ISO, 1996] and relevant to $H_p(10)$ dosimetry. The quality of the resulting response characteristics are judged relative to various international, European and UK criteria, as discussed below.

2.1.1 International Standards

Accuracy requirements for personal dosemeters are generally based on the factor prescribed by ICRP for individual monitoring [ICRP, 1997], which is 1.5 at the 95 % confidence level. This stipulation is similar to that of ICRU for instrumentation, and is usually considered to apply to the quantity being measured, i.e. $H_p(10)$ or $H_p(0.07)$. The factor of 1.5 is adopted in both ISO and IEC standards.

In the IEC standard on performance requirements for thermoluminescence dosimetry systems [IEC, 2006], the factor of 1.5 is applied to the calibration factor (i.e. the reciprocal of the response characteristic). This becomes a range of -29 % to +67 %, at the 95 % confidence level, for the $H_p(10)$ response characteristic in the stated energy range of use and at angles up to 60° to the normal (or a higher angle if desired). The IEC requirements for the $H_p(10)$ photon response include: an energy range of at least 80 keV to 1.25 MeV; a limit of 1.2 on the relative response for lateral irradiation; and a limit on the unwanted electron response of 10% of the true $H_p(0.07)$ value for 800 keV electrons (corresponding to the mean energy of emission from $^{90}Sr/^{90}Y$). The last criterion may be paraphrased as: the $H_p(10)$ response in a $^{90}Sr/^{90}Y$ field should be no more than 0.1 times the $H_p(0.07)$ response in that field, assuming that the $H_p(0.07)$ estimate is correct [IEC, 2007].

It is proposed that the HPA design should meet the IEC accuracy requirements for the energy range from 15 keV to 7 MeV, and adopt a maximum electron energy of 2 MeV for the 10 % limit on unwanted $H_p(10)$ response. This limit is based on the range of electrons in tissue: a 2 MeV electron travels about 10 mm in tissue, so lower energy electrons should not penetrate the filter and reach the detector element. The IEC standards are not mandatory in the UK at present, but are frequently used as a guide by manufacturers and users.

2.1.2 European Recommendations

The EC recommendations [EC, 1994] for the energy and angle dependence of personal dosemeters required the relative response averaged over the angles 0°, 20°, 40° and 60° to be approximately within the range 0.6 to 1.4, at each energy and at the 95 % confidence limit. The EC recommendations have recently been revised [EC, 2009], but are compatible with the international standards.

2.1.3 UK Requirements

The Health and Safety Executive (HSE) requires that the dosemeter can be shown to be suitable and reliable, and have a consistent and adequate performance for the radiation fields and environments in which it will be used [HSE, 2008]. For the HPA dosemeter to be offered for general use, the highest dosimetric standards will therefore need to be met. Assessment is achieved by type-testing and field trials.

2.2 Design Specifications

The Harshaw TLD-700H 'card' may be seen in Figure 1(a). It effectively comprises doped lithium fluoride crystals (LiF:Mg,Cu,P, or often simply 'LiF' in this document for brevity) sandwiched between two polytetrafluoroethylene (PTFE or 'Teflon®') sheets, themselves sandwiched between two riveted aluminium plates, with 10 mm diameter 'clearance' holes cut into the metal around the LiF. Only two LiF detectors are used in the HPA TLD system out of a possible four, one for each depth dose assessment. The LiF disks are identical, apart from their thicknesses: the $H_p(10)$ detector is 0.38 mm thick, the $H_p(0.07)$ is 0.25 mm thick. Viewed from face-on (i.e. looking towards the body), the card resembles a rectangle with one of its corners 'missing'; it was decided that this shall be placed at the bottom-right of the device, with the $H_p(10)$ and $H_p(0.07)$ detectors located in the bottom-right and bottom-left positions respectively (labelled as positions '2' and '3' by the manufacturer). The entire card is placed inside a thin, optically opaque wrapping comprising of two 12 μm thick polyethylene terephthalate (PET) layers and one 38 μm thick ethylene vinyl acetate (EVA) layer, the crimping of which (not shown in Figure 1(a)) extends several millimetres beyond the ends of the card.

The holder was to be constructed from polypropylene (PP) of thickness 2 mm. It was to be designed to just fit the wrapped card, such that the card is held rigidly in place relative to the holder. In effect, the PP provides a 2 mm thick covering around the entire card/filter system, apart from a hole in front of the $H_p(0.07)$ detector location, and a viewing window though which the card's label may be read.

To calibrate, the holder was placed on the front face of a water-filled ISO slab phantom of dimensions $300 \times 300 \times 150$ mm^3 [ISO, 1989; Alberts *et al*, 1994; Kramer *et al*, 1994]. The phantom walls were constructed from polymethyl methacrylate (PMMA or 'Perspex®'); the front 300 x 300 mm^2 wall was 2.5 mm thick, and the remaining walls were of thickness 10 mm.

The MCNP rendering of the overall configuration is seen in Figures 1(a) - (c). Figure 1(a) shows the card positioned inside a holder, with both the front face and wrapper front removed. Figure 1(b) shows the front face view of one of the possible designs of holder. Almost all of the designs investigated in this work had a basic geometry similar to that illustrated in Figure 1(b), with the majority of changes focussing solely on the $H_p(10)$ filter details, as will be seen in due course. Figure 1(c) shows a cross-section of the same design along a plane through the centres of the two detectors and perpendicular to the phantom face. The phantom extends well beyond the boundaries of the figure.

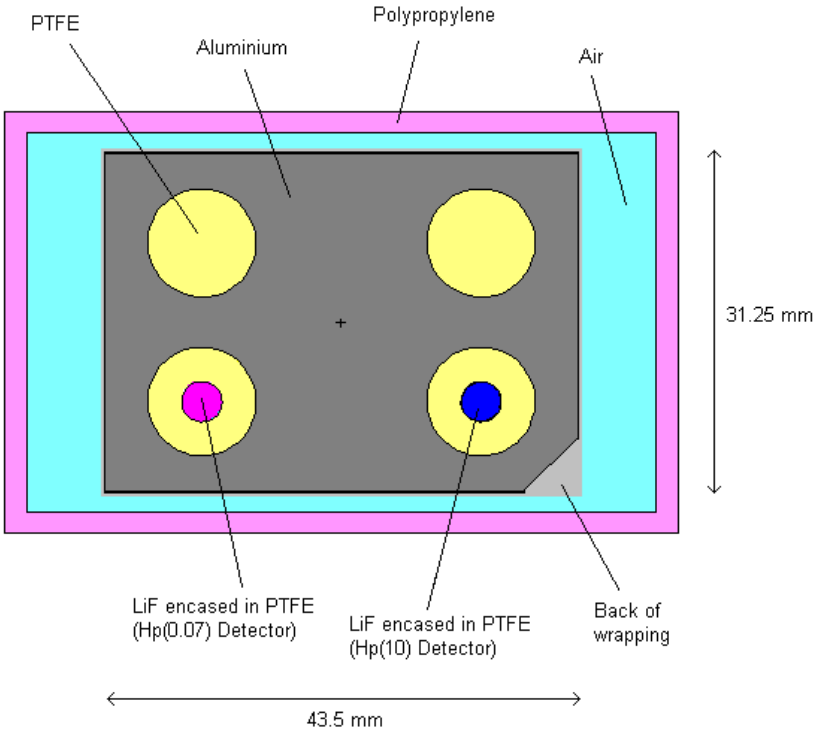

Figure 1(a): The Harshaw TLD-700H card in its holder. The front of the holder and the front half of the wrapper have been removed for ease of viewing.

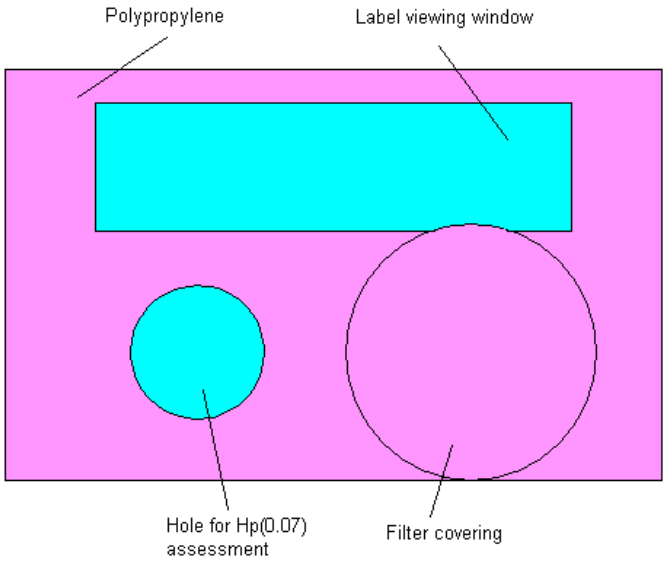

Figure 1(b): Front-face view of a holder design. This design features a hole located in front of $H_p(0.07)$ element, and a 4.3 mm thick PTFE disk filter of diameter 18 mm, covered by polypropylene of thickness 2 mm, located in front of $H_p(10)$ element.

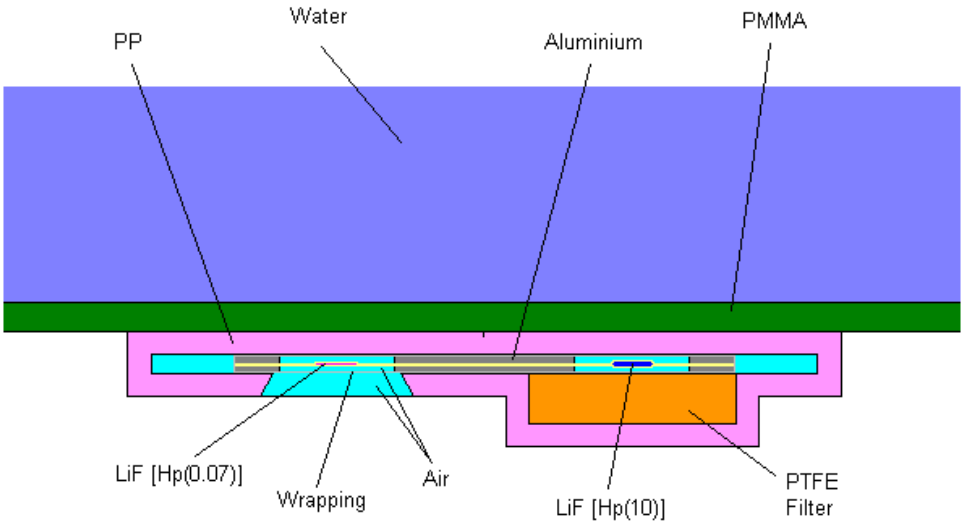

Figure 1(c): Cross-sectional view of a dosemeter device on the front-face of the phantom. The view is in a horizontal plane that is through the centres of the two LiF elements and perpendicular to the phantom front-face. The design shown incorporates a 4.3 mm thick PTFE disk filter of diameter 18 mm, centred in front of the H_p(10) element. The hole in front of the H_p(0.07) detector is frustum-shaped, with a top diameter of 12 mm and a bottom diameter of 15 mm. Only a small portion of the phantom is visible.

2.3 MCNP Simulation

Throughout the entire design stage of the TLD, MCNP version 4c2 [Briesmeister, 2000] was used to simulate particle transport through the configuration; the potential impact of instead using the newer package, MCNP5, is considered later. The types of geometry featured in Figures 1(a) - (c) were specified relative to an origin placed at the centre of the front face of the phantom, with the centre of the card positioned on the line perpendicular to the phantom at this point. The front of the phantom, back of the holder, front and back of the card, and the holder front were all parallel.

The source was defined as a plane-parallel beam, centred on the origin, with a circular cross-section of radius 220 mm (i.e. sufficient to cover the entire front-face of the phantom, for which the centre-to-corner distance is ~212 mm). The beam made an angle of θ to the phantom front surface normal, with horizontal beams that impinge from the left (viewed from face-on, i.e. the H_p(0.07) detector 'side') labelled by positive angles, and from the right (i.e. the H_p(10) side) by negative angles. In the context of this report, 'horizontal' is taken to imply that, in the laboratory frame-of-reference, the velocity vectors of the source photons are constrained within planes that are parallel to the plane that is: 1) perpendicular to the phantom front face; and 2) passes through the centres of the two LiF elements.

Generally, photon-only transport was employed throughout this work to evaluate the devices' performances, with use made of the kerma approximation. A more realistic, yet more complicated and hence more time-consuming, full-electron/photon transport mode simulation of the set-up may follow in the future; a few basic electron/photon

calculations were, however, performed to confirm some of the parameters of the final design, as discussed later. The entire TLD-phantom configuration was surrounded by vacuum, and the source particles were set as photons. Specifically, the ISO Narrow Series X-ray spectra [ISO, 1999] provided by Physikalisch Technische Bundesanstalt (PTB) [Ankerhold, 2000] were used as the input source fields, along with: monoenergetic 661.661 keV photons corresponding to a ^{137}Cs source; an equal-proportion distribution of 1173 keV and 1333 keV photons corresponding to a ^{60}Co source; monoenergetic 4440 keV photons corresponding to the $^{12}C(p,p'\gamma)^{12}C$ reaction (referred to in ISO 4037 as R-C [ISO, 1996; ISO, 1999]); and a distribution of 6130 keV, 7717 keV and 6917 keV photons in the ratio 194:5:1 corresponding to the $^{19}F(p,\alpha\gamma)^{16}O$ reaction (R-F) [ISO, 1996]. Note that when referring to an x-ray field or source throughout this report, the quoted value *E* keV represents the energy that corresponds to the weighted mean of that distribution. Thus, the '16 keV source', for example, relates to the ISO N-20 distribution. Note also that for data analysis purposes, such as graph plotting, the cobalt source was assumed effectively equivalent to a monoenergetic 1253 keV source, and the R-F to a 6174 keV source.

The doses in the two LiF disks were evaluated using MCNP '*f6:p* tallies'. These provide a track length estimate of the energy deposition, in MeV/g per source particle, averaged over a cell, where the 'cell' here is defined as the detector element of interest. The relative response, $R(\theta,E)$, of the detector to the given energy source was then calculated from the kerma relationship:

$$R(\theta,E)=\left[\frac{\left(D(\theta,E)_{LiF}\Big/D(0,E)_{Air}\right)\times\dfrac{1}{k(\theta,E)}}{\left(D(0,Cs)_{LiF}\Big/D(0,Cs)_{Air}\right)\times\dfrac{1}{k(0,Cs)}}\right]\times\frac{\eta(E)}{\eta(Cs)} \qquad (1)$$

where:

- $D(\theta,E)_M$ is the dose or, equivalently here, kerma per-source-particle (i.e. the *f6:p* tally) in the detector of interest, for detector material *M* (i.e. LiF or air), for a source field of energy *E,* impinging at θ°;
- $k(\theta,E)$ is the air kerma conversion coefficient at that energy and angle for the relevant dose quantity (i.e. $H_p(10)$ or $H_p(0.07)$);
- and $\eta(E)$ is the intrinsic efficiency of the lithium fluoride detector at source energy *E*.

The efficiency function is effectively a 'bridge' between experimental and calculated results, the values for which were obtained from theory and previous work, as is elaborated upon later.

For the Narrow Series, the energy-distribution-weighted air kerma to $H_p(10)$ conversion coefficients obtained from the work of Ankerhold [Ankerhold, 2000] were used for the $H_p(10)$ response, in order to provide consistency with the source fields. These conversion coefficients differ from those in ISO 4037-3 [ISO 1999], especially at low energies (33 keV and below) where they become particularly sensitive to small changes in the photon energy distribution at the position of the dosemeter. For $H_p(0.07)$, no Narrow Series conversion coefficients were supplied by Ankerhold that correspond to a slab phantom. For $H_p(0.07)$, it was therefore decided that the Ankerhold rod phantom

conversion coefficients would be used at 16 keV and 20 keV, with the 30° and 60° values set the same as the 0° coefficient in each case, due to a lack of a better alternative. For the remainder of the Series, however, slab phantom data from ISO 4037-3 [ISO, 1999] were employed to calculate $H_p(0.07)$, with $k(\theta,E) \neq k(\theta',E)$. These decisions represented what were thought to be the best compromises under the circumstances, taking factors such as anticipated measurement conditions and photon backscatter into account [Eakins 2006, Eakins *et al*, 2007]. For all energies, it was assumed that $k(-\theta,E) = k(\theta,E)$. For the 662 keV, 1253 keV, 4440 keV and 6174 keV sources, ISO conversion coefficients were used for $H_p(10)$. Moreover, at these high energies, the $H_p(10)$ conversion coefficients were also used to determine the $H_p(0.07)$ response, due to a lack of any more appropriate data; this was not expected to introduce any significant error into the results, however. Note that the mean energy quoted in ISO 4073-3 for the R-F source is 6610 keV, not 6174 keV; this difference was also not thought likely to cause a problem for the present purposes. As is evident from Equation (1), all results were normalized to the 0° incidence response for caesium irradiation.

In order to calculate the air doses, the simulations were repeated with the materials of the phantom, holder and LiF/card arrangement all set to air of density 0.00120484 g/cm^3 and mass composition: 75.5267 % nitrogen, 23.1781 % oxygen, 1.2827 % argon and 0.0124 % carbon. The doses tallied in the new 'air detectors' (i.e. what had previously been the LiF cells) gave the required $D(\theta,E)_{air}$. In practice, this procedure was only performed once for each energy distribution during the entire course of the investigation, with the assumption then made that minor changes to the holder design, and different angles of irradiation, would only affect the outcome negligibly.

To improve computational efficiency, MCNP '*importances*' were increased in the cells surrounding the LiF. This setting followed the general 'rule' that the importance of line-of sight cells tends to rise exponentially (base 2) with proximity to the tallied region. In the majority of the simulations featured in this report, reliable statistics were achieved by running 10^8 starting photons, which corresponded to approximately one hour of computer time on a 2.67 GHz Pentium® 4 desktop machine. The effects of both cell importances and starting particle numbers ('*nps*') were investigated in a short series of preliminary trials.

Default MCNP input options (e.g. Thick Target Bremsstrahlung, coherent scattering, MCNP-style 'bin-centred' energy indexing, etc.) were used in all simulations reported, unless otherwise stated.

Typical MCNP input files for the configurations are given in Appendices B - D. Appendix B is the input file used for the determination of the air kerma result at 16 keV. Appendix D is the input file describing the final TLD design.

3 PRELIMINARY WORK AND REMARKS

The physics and use of doped LiF in TLD devices is described elsewhere (see [McKinlay, 1981], amongst others), so it is not the intention to enter into such a

discussion in this report. Neither is it intended to concentrate on any of the previous expositions into the redesign process, though due reference is made to the contributions of César Molinos Solsona [Molinos *et al*, 2004] during his work within the External Ionizing Radiation Dosimetry Group of the former NRPB, for example in comparing the performances of copper against aluminium as an $H_p(10)$ filter. Technical discussions of the methodology and operation of the MCNP algorithm are also omitted [Briesmeister, 2000].

3.1 Filter alternatives

Before deciding upon the filter material for the $H_p(10)$ dose assessment, a number of alternative possibilities and arrangements were investigated. In chronological order, these were:

a A 0.59 mm thick aluminium disk of radius 7.475 mm, covered by 2 mm PP[A];
b A 0.7 mm thick aluminium disk of radius 7.475 mm, covered by 2 mm PP;
c A 0.7 mm thick aluminium disk underneath a tin disk, both of radius 7.475 mm, all covered by 2 mm PP. Tin disks of thicknesses 0.1 mm, 0.05 mm, 0.025 mm and 0.01 mm were trialled;
d A 0.7 mm thick carbon disk of radius 7.475 mm, covered by 2 mm PP;
e A 0.59 mm thick filter disk of 'Dural®' type aluminium (95 % Al, 4 % Cu, 1 % Mg), radius 7.475 mm, covered by 2 mm PP;
f A 0.7 mm thick filter disk of 'Dural®' type aluminium, radius 7.475 mm, covered by 2 mm PP;
g A 0.59 mm thick aluminium disk filter of radius 7.475 mm, covered by a thick polypropylene dome of profile similar to that used in the previous TLD holder design;
h A 0.7 mm thick aluminium disk filter of radius 7.475 mm, covered by a thick polypropylene dome of profile similar to that used in the previous TLD holder design.

Mixed success in varying proportions was reported with these suggestions, with the 0.7 mm thick, standard aluminium disk covered by 2 mm PP design (‘*h*’, above) emerging as the strongest contender. Eventually, however, all of these proposals were discarded, as it was shown that they could all potentially run into significant problems when electrons are considered as part of the source field. Essentially, 0.7 mm of aluminium would not adequately prevent even 1 MeV electrons from reaching the $H_p(10)$ detector, and this could seriously undermine the device’s performance. The above suggestions will therefore not be discussed beyond this section of the report, save to say that despite these problems it was the 0.7 mm aluminium disk configuration, but with all materials set to air, that nevertheless provided the air kerma data used throughout the design project, as detailed in Appendix B.

[A] The filter covering in designs ‘*a*’ to ‘*f*’ was actually slightly spherically concave, with a thickness at its outer edge of 2.15 mm, and a thickness at its centre of 1.9 mm. However, an ‘average’ value of 2 mm is quoted for convenience.

3.2 Source Field

The ISO Narrow Series X-ray spectra supplied by PTB were used throughout the design programme. This, however, presented a problem: PTB provide data for source fields at distances of 1 m and 2.5 m, whereas the HPA Radiation Metrology Group utilizes a source field located at a distance of 2 m from the phantom front. Because MCNP and experimental data were ultimately to be compared, the possible effects of such differences needed to be established.

Using the configuration described in '*a*' of Section 3.1, the transport was simulated at energies of 16 keV, 20 keV, 24 keV, 33 keV, 48 keV and 662 keV using both 1 m and 2.5 m PTB source data. The doses acquired by the detectors (MCNP '*f6:p*' tally) using these alternative distance datasets were then compared at each energy. The result was that the differences in dose between the two cases were all less than the one standard deviation MCNP statistical uncertainty, which was approximately 3 %. The average absolute difference was less than 1 %, with the greatest difference occurring at 16 keV where the 2.5 m result was about 2.5 % larger than its 1 m counterpart. Moreover, no general trend was observed in these discrepancies across this energy range, suggesting that any apparent differences were just due to stochastic effects.

It is therefore suggested that a source field at 2 m would not be greatly different in effect from a source field at either 1 m or 2.5 m. Moreover, given that the differences generated by using one of these two sets of PTB data instead of the other appear negligible, it should not matter significantly which is employed. Hence, and because the 2.5 m data seem intuitively to be the most natural choice to represent the actual 2 m situation, only the 2.5 m source fields were used in the subsequent work.

3.3 Efficiency Function

The function $\eta(E)$ required to evaluate the response represents the intrinsic efficiency of the real LiF detector set-up. That is, $\eta(E)$ attempts to take account of all of the physical processes that prevent the light measured by the card reader from being directly proportional to the dose deposited in the LiF, independent of the energy of the incident radiation. Included in $\eta(E)$, then, are factors linked to:

a Photomultiplier/reader efficiency;
b Non-tissue equivalence of lithium fluoride: the energy deposited in a small element of lithium fluoride will exhibit a different energy dependence compared to the energy deposited in a small element of tissue;
c Self-attenuation of the lithium fluoride: the efficiency with which the light escapes from the lithium fluoride will depend on the depth-dose profile within the lithium fluoride chips.

Efforts have been made elsewhere to determine $\eta(E)$ on theoretical grounds. One such attempt was by Olko *et al* ([Olko *et al*, 1999] and references therein, e.g. [Olko, 1996]) who used a phenomenological approach based on Monte Carlo techniques and the 'Microdosimetric One-Hit detector model' to suggest the energy dependence of the efficiency function for LiF:Mg,Cu,P in the form of MCP-N® pellets. However, another way

of estimating this parameter is by making a simple comparison between MCNP and experiment. Specifically, the value of $\eta(E)$ may be determined from Equation (1) by equating $R(\theta,E)$ to the measured response, and dividing by the square-bracketed term obtained from MCNP.

In practice, both methods were required in the current program of research. In the early stages of the investigation, no experimental data were available, so the theoretical results of Olko *et al* were used in order to obtain the TLD response. But, as measured data did become available (initially, from 'a' and 'b' in Section 3.1 above), it was possible to perform the 'comparison process' and save the results for use in subsequent calculations. The question then became: how exactly should the experimental and theoretical data be used? Of course, this is a potentially hazardous issue. On the one hand, an obvious question arises as to the accuracy and appropriateness of Olko's MCP-N based model to the situation under analysis here. On the other, solely using the new MCNP data runs the risk of propagating both systematic and statistical errors, and also has the undesirable problems associated with the fact that the data set of available experimental results is at some energies limited to a single member. So overall, neither the theoretical nor the comparison approach is considered wholly satisfactory, and it should therefore be noted that the use of the efficiency function represents arguably the greatest source of uncertainty in all of the response results presented in this report.

TABLE 1 Interim efficiency function, $\eta_{interim}$.

Energy (keV)	Olko *et al* Efficiency	*N*	η_{interim}
16.3	0.675	7	0.763
20.2	0.75	7	0.732
24.5	0.775	7	0.749
33	0.8	7	0.785
48	0.8	7	0.786
65	0.775	2	0.666
83	0.75	2	0.673
100	0.775	2	0.689
118	0.8	2	0.734
161	0.85	2	0.762
205	0.9	2	0.824
248	0.925	2	0.857
662	1.0	2	1.000

In the end, the outcomes of the comparison procedures for the 0.59 mm and 0.7 mm thick aluminium filter data were averaged, along with the theoretical results of Olko *et al*, to provide a first approximation for the desired function. Explicitly, for a given energy E, the average efficiency was given by:

$$\bar{\eta} = \frac{1}{N}\left(\eta_{\mathrm{O}} + \sum_{t}\sum_{\theta}\eta\right)$$

where η_O is the Olko result, t is the filter thickness (= 0.59 or 0.7), irradiation angle θ=0°, 30° or 60°, and N is the number of data points available at that energy (noting that data were not available for every angle for each thickness). The resulting average function, labelled $\eta_{interim}$, is shown in Table 1.

Clearly, (N-1) is the number of data points determined from the present investigation by using the MCNP/experiment-comparison method; only for the 0.7 mm Al filter with the source at normal incidence were measurement data obtained for the entire range of ISO energy distributions. Standard deviations in experimental results were approximately 2-4 %, and in MCNP less than 5 %. Uncertainties in the Olko *et al* values were not provided.

3.4 PP Thickness Variation

The configuration considered in '*b*' of Section 3.1 involved a filter comprised of a 0.7 mm thick aluminium disk behind a 2 mm thick polypropylene covering. Even though this suggestion was not pursued further as a potential design, it is still valid to question the tolerance of such a device's performance to variations in the thickness of the PP. Such an issue is important, not only to account for possible variations caused by the manufacturing process, but also because it was proposed to emboss the front of the filter cover of the final holder design with a relief of the HPA logo. Accordingly, the PP covering was likely to be up to an additional 0.25 mm thick in places, and so determining whether or not this would impede device performance was crucial.

To overestimate this potential effect, an exaggerated worst-case scenario was defined and simulated that involved a TLD configuration featuring a filter of 0.7 mm thick aluminium covered by 3 mm PP. The results were then compared with the response of the similar design that featured only a 2 mm thick PP cover in front of the aluminium disk (i.e. '*b*'). Only normal incidence exposures were considered. As was to be expected, it is the response to 16 keV sources that was worst affected by the increased thickness. But, even here the dose deposited in the detector was only 4 % less in the 3 mm thick case than in the 2 mm case. This compares with a relative error (one standard deviation) in the result of approximately 3.5 %. Moreover, for most of the rest of the Narrow Series energy range, the percentile differences between the two cases were less than 1 %.

Assuming linearity, it is therefore suggested that deviations in the PP thickness of about 0.25 mm from the usual 2 mm would be expected to lead to negligible discrepancies in the response of the device. Indeed, any differences that might arise would be irresolvable within the uncertainty estimates quoted for the response.

4 THE PTFE SLAB FILTER

The proposal of central importance to this report was to use a PTFE filter in front of the $H_p(10)$ element, covered by PP. Because mass-stopping-power depends on the number of electrons per unit mass, a greater mass-thickness is required for the PTFE than for

the PP. A filter consisting of 3.7 mm PTFE (density 2.2 g/cm^3) covered by 2 mm PP (density 0.9 g/cm^3) was suggested initially, as this corresponds to a surface density, σ, of:

$$\sigma = (0.37 \times 2.2) + (0.2 \times 0.9) = 0.994$$

which is roughly equal to 1 g cm^{-2}, as necessary to emulate 10 mm of ICRU tissue [ICRU, 1980], assuming 'plastic' can be taken as being approximately tissue equivalent. Indeed, PTFE is likely to be far more tissue-equivalent than aluminium, which was used in the 'old' holder design: the old filter consisted of 8 mm polypropylene (PP) plus 0.7 mm aluminium [Shaw, 1977], which corresponds to an areal density of ~910 mg/cm^2, equivalent to only 9.1 mm of 1 g/cm^3 material.

In order to evaluate the performance of such a PTFE + PP filter, a device of the type shown in Figure 2 was considered. The PTFE filter was a slab of dimensions 43.6 $\times$ 31.4 $\times$ 3.7 mm^3, with its height and width chosen such that it covered the entire card, practically filling the extent of the holder. A 55.6 $\times$ 43.2 $\times$ 2 mm^3 slab of PP then covered the PTFE, acting as the front of the device; from the exterior, the holder approximately resembled a solid block of polypropylene. Both an MCNP and an experimental study of the configuration were undertaken.

The normal incidence results for the slab filter TLD are shown in Figure 3(a). The low energy results at 0°, 30° and 60° are seen in Figure 3(b). The MCNP responses were calculated using the values of the efficiency function $\eta_{interim}$ given in Section 3.4. In all cases, the calculated responses are considered acceptable, being reasonably flat and close to unity, demonstrating the effectiveness of PP+PTFE as an $H_p(10)$ filter.

By comparing the raw MCNP data with experimental measurements, and using Equation (1), a new set of LiF efficiency data could be produced. Moreover, by taking the mean of these results with those comprising $\eta_{interim}$, an improved version of the average efficiency function was obtained for use in subsequent calculations. This latest function, referred to as *Eff-July05* and labelled $\eta_{Eff\text{-}July05}$, is summarised in Table 2, where the square-bracketed values indicate the number of data points available at that energy. Note that by containing more experimental data than $\eta_{interim}$, the function $\eta_{Eff\text{-}July05}$ is assumed more accurate. As a consequence, it was $\eta_{Eff\text{-}July05}$ that was used in all ensuing determinations of the TLD response presented in this report, unless stated otherwise.

TABLE 2 Improved efficiency function, $\eta_{Eff\text{-}July05}$

Energy (keV)	**16.3** [10]	**20.2** [10]	**24.5** [10]	**33** [10]	**48** [10]	**65** [2]	**83** [2]
Efficiency	0.766	0.728	0.747	0.773	0.771	0.721	0.712
Energy (keV)	**100** [3]	**118** [2]	**161** [2]	**205** [2]	**248** [2]	**662** [3]	**1253** [1]
Efficiency	0.725	0.767	0.806	0.862	0.891	1.000	1.014

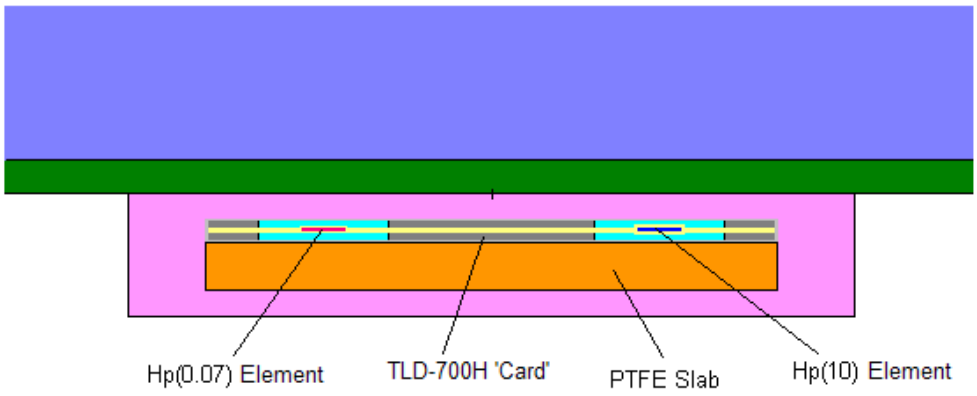

Figure 2: Cross-sectional view of the configuration used to investigate the performance of a PTFE slab filter. The view is in a plane through the centres of the two LiF elements, perpendicular to the phantom face. Only part of the phantom is shown.

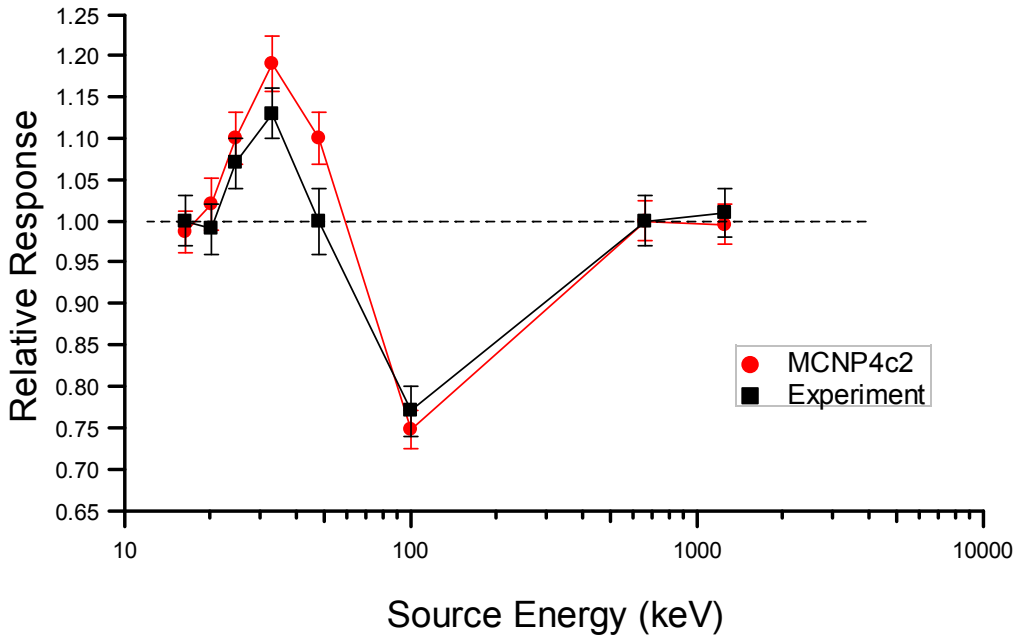

Figure 3(a): MCNP4c2 and measured $H_p(10)$ relative responses of a TLD configuration that featured a 3.7 mm thick PTFE slab filter, exposed to sources at normal incidence. The interim efficiency function, $\eta_{interim}$, was used.

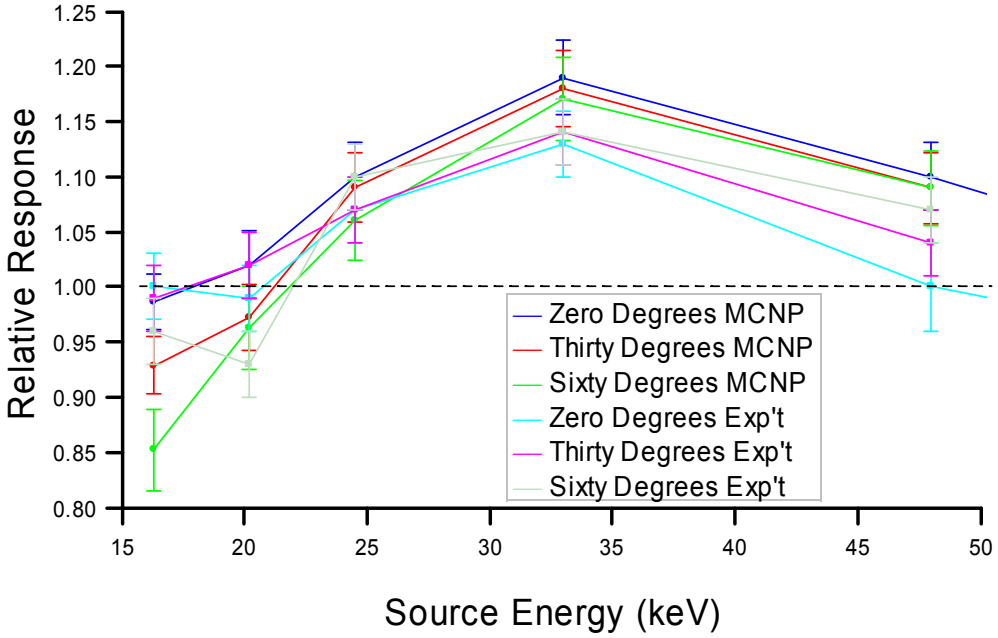

Figure 3(b): MCNP4c2 and measured $H_p(10)$ relative responses of a TLD configuration that featured a 3.7 mm thick PTFE slab filter, exposed to low-energy source fields at 0°, 30° and 60° incidence. The interim efficiency function, $\eta_{interim}$, was used.

5 THE 3.73 MM PTFE DISK FILTER

With the above agreement between MCNP and experiment validating the calculation procedure, and with the suitability of PTFE demonstrated, attention turned towards optimizing a TLD device that incorporated such a filter. Following on from previous work, a slightly thicker filter of 0.373 cm was used initially, providing a surface density closer to 1.00 g/cm^2 when covered by 0.2 cm of PP (that is, 0.373×2.2 + 0.2×0.9 = 1.0006 g/cm^2).

Clearly, a slab filter of the type described in Section 4 is impractical if $H_p(0.07)$ doses are to be determined. More than this, however, even if the filter is not directly in front of the $H_p(0.07)$ element (viewed from face-on), it is still possible that some potential designs might result in it 'shadowing' this detector, especially at high angles of incidence. So, partly in an attempt to avoid such effects, the PTFE filter was constrained to a disk centred in front of the $H_p(10)$ chip. Such an arrangement is similar to the configuration illustrated in Figures 1(a) - (c). An immediate question is: what disk diameter may be used to provide an acceptable $H_p(10)$ response from 0° to (horizontal) 60° angles of incidence, without affecting the $H_p(0.07)$ response?

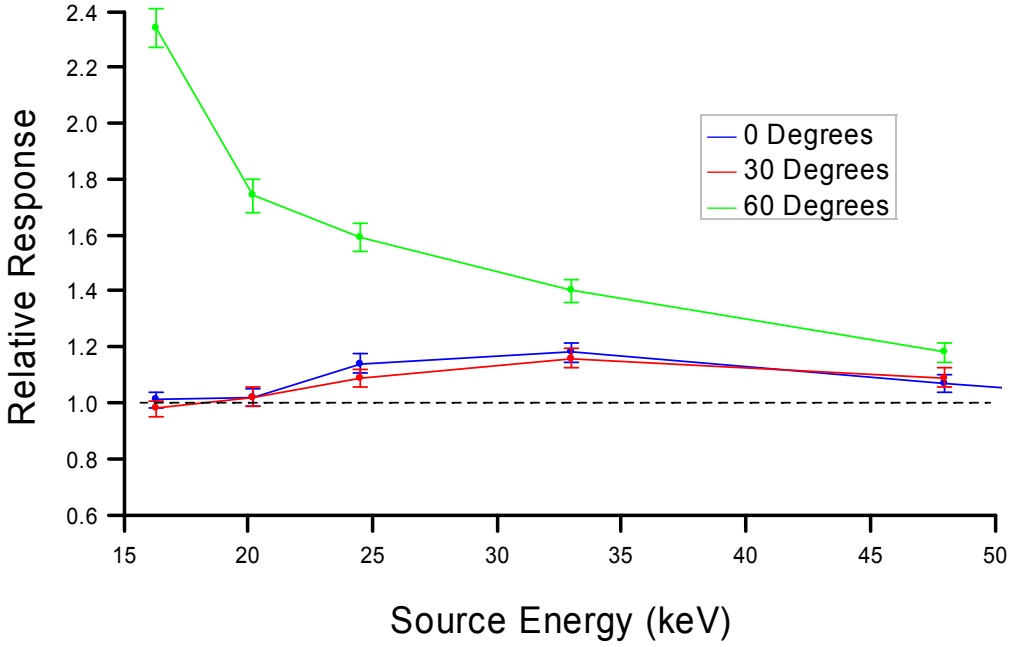

Figure 4: MCNP4c2-calculated $H_p(10)$ relative responses of a TLD configuration containing a 3.73 mm thick, 10 mm diameter PTFE disk filter, for low-energy Narrow Series source fields at 0°, -30° and -60° incidence. The interim efficiency function, $\eta_{interim}$, was used.

In the first instance, a disk of diameter 10 mm was employed. The $H_p(10)$ results for this dosemeter at low source energies are shown in Figure 4. Note that these were incident at negative angles: the source impinged from face-on right, i.e. from the $H_p(10)$ 'side' of the device, in preparation for later work investigating any 'shadowing' of the $H_p(0.07)$ detector by the PTFE lump. Note also the use of $\eta_{interim}$ to calculate these results. Although reasonable performance is reported at horizontal source incidence angles of 0° and -30°, the device clearly over-responded at -60°. This was suggested to be a geometrical effect. Specifically, it is thought that at -60° the source beam is 'missing' some of the filter: some of the particles enter the PTFE from its side. The photons consequently arrive at the LiF comparatively unattenuated, thereby depositing too great a dose. At zero and thirty degrees incidence, most of the detected photons were incident on the front of the filter, so this effect does is not significant, leading to an acceptable performance at these angles. The situation is illustrated in Figure 5.

In an attempt to overcome the above problem, 14 mm and 17.92 mm diameter disks were investigated. A diameter of 14 mm was considered because, for the 'old' holder design [Shaw, 1977], it represents about the maximum diameter of PTFE disk that could be used such that the covering layer of PP would be no less than 2 mm from the edge of the holder. Similarly, a 17.92 mm disk (henceforth referred to as 18 mm, but see Appendix A) represents a scenario in which the edge of the filter cover would just touch this boundary. The $H_p(10)$ and $H_p(0.07)$ relative responses of these two designs are shown in Figures 6(a) and 6(b) respectively, derived using the new efficiency function,

$\eta_{Eff\text{-}July05}$. Only -60° incidence angles were investigated, with the assumption made that the 0° and -30° results would not differ significantly from the case of the 10 mm diameter disk. As can be seen, although the 14 mm filter was an improvement on the 10 mm design, it still appears that some 'missing' occurred, which is to be expected from the earlier argument regarding geometry (Figure 5). With an 18 mm filter, however, adequate filtration was achieved, consistent with the theory that most of the detected photons were now striking the larger diameter PTFE disk on its front circular face rather than its side. In neither case did shadowing of the $H_p(0.07)$ detector by the PTFE+PP filter appear to be a problem: as expected from a consideration of the geometry shown in Figure 1(c), it was found that the responses of this detector were unaffected by the different diameter filters modelled.

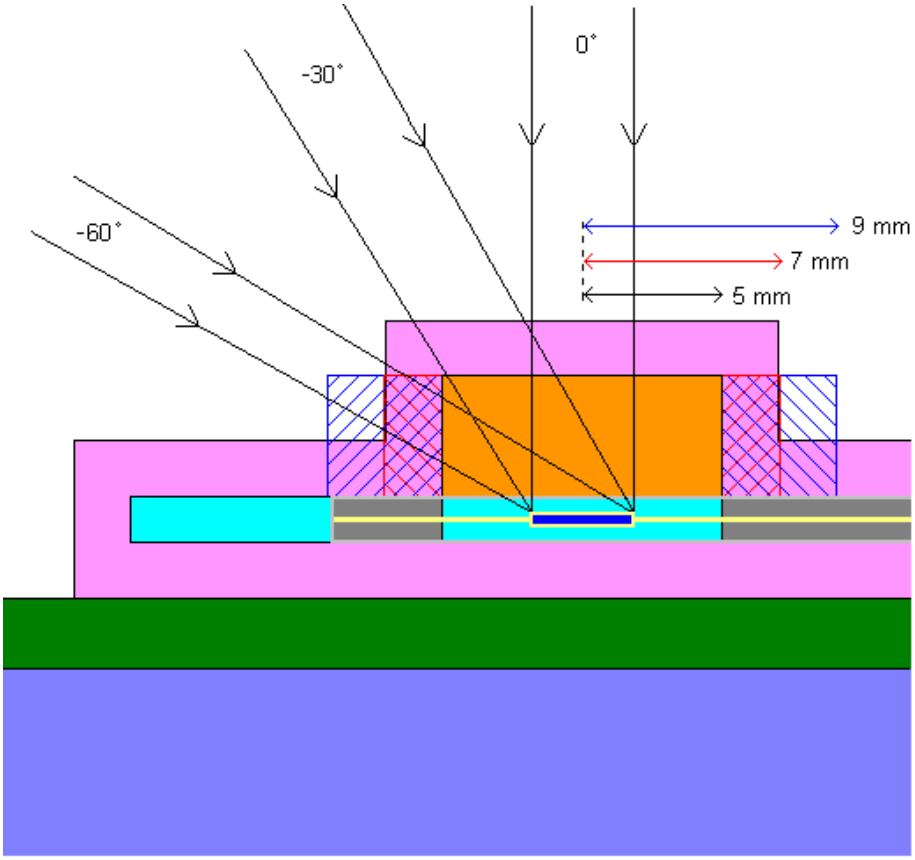

Figure 5: Schematic illustration of the irradiation of a TLD device containing a 3.73 mm thick PTFE disk filter. With a disk diameter of 10 mm (orange region), photons from a source at -60° impinge onto the side of the PTFE filter on their way to the LiF $H_p(10)$ element, and are hence insufficiently attenuated. For a 14 mm diameter filter (red hashed region), some of the photons strike the PTFE's top surface, but many still impinge on its side. For an 18 mm diameter disk (blue hashed region), most of the photons now strike the top of the filter, as desired. In all cases, adequate filtration appears to be provided for exposures at both 0° and -30°. Note that in both the 14 mm and 18 mm diameter cases, the PP covering would be extended appropriately to envelop the filter, just as it is shown to do above for the 10 mm case (pink region), but for clarity these alterations have not been shown in the figure.

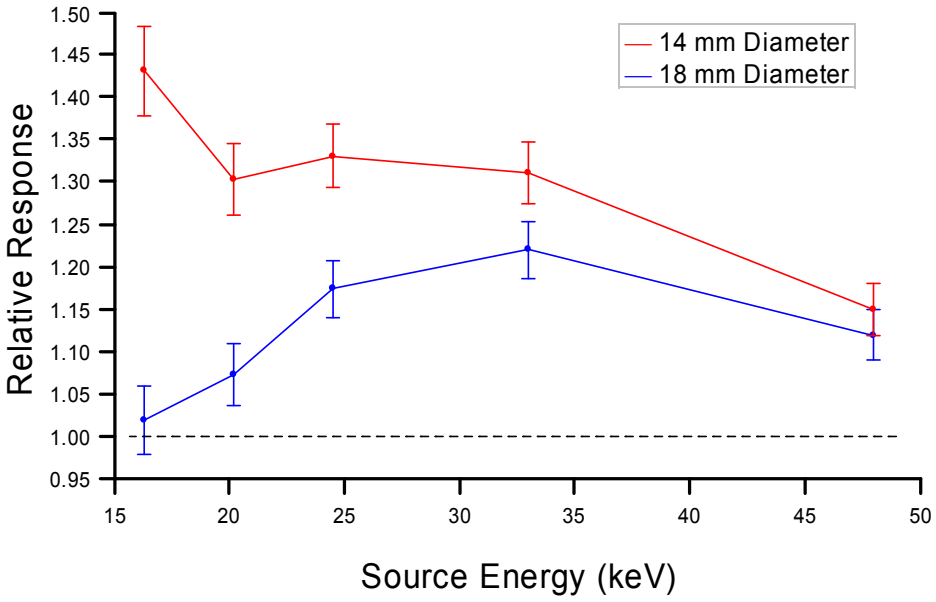

Figure 6(a): MCNP4c2-calculated $H_p(10)$ relative responses of a TLD with a 3.73 mm thick PTFE disk filter, for low-energy source fields at -60° incidence. 14 mm and 18 mm diameter disks are compared. Efficiency data from $\eta_{Eff\text{-}July05}$ were used.

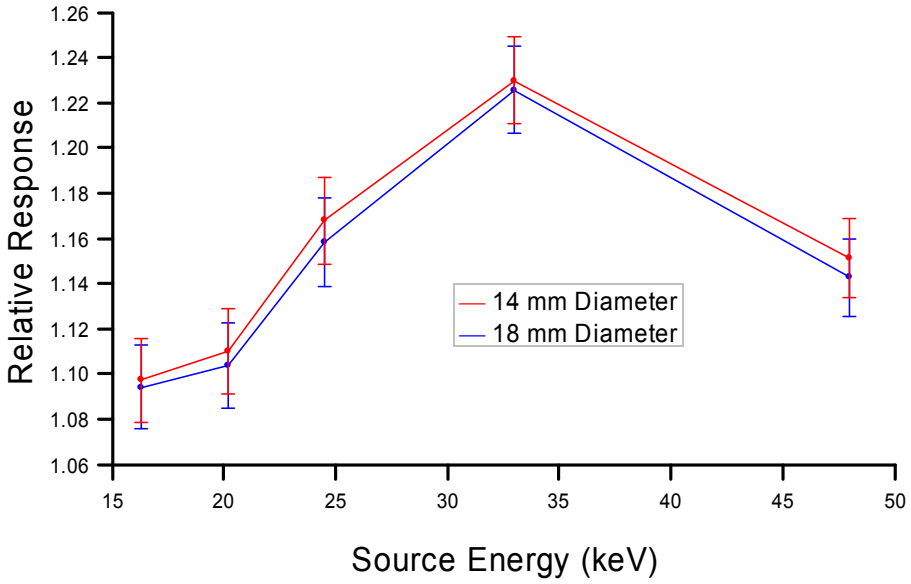

Figure 6(b): MCNP4c2-calculated $H_p(0.07)$ relative responses of a TLD with a 3.73 mm thick PTFE disk filter, for low-energy source fields at -60° incidence. 14 mm and 18 mm diameter disks are compared. Efficiency data from $\eta_{Eff\text{-}July05}$ were used.

6 THICKER DISKS

Although Figures 6(a) and (b) indicate some success, with fairly flat relative response profiles exhibited for the 18 mm diameter, 3.73 mm thick PTFE filter configuration, it is clear that the performance of the device could nevertheless be improved further. In particular, it is noted that both the $H_p(10)$ and $H_p(0.07)$ responses are reasonably high, nowhere, in fact, dropping below unity within the energy region studied. In order to reduce this general over-response, greater thicknesses of PTFE are required, to provide more attenuation. Moreover, such a change would also help when electrons are considered as part of the source field: due to the relationship between an electron's energy and its range in a material, increasingly thicker filters can stop electrons with increasingly higher energies from reaching the detector. To these ends, 4 mm and 4.3 mm thick disks were investigated, which correspond to the ranges of 1.9 MeV and 2.0 MeV electrons respectively[B]. Disk diameters of 18 mm were again used, due to the acceptable angle response that had already been demonstrated.

Figures 7(a) and (b) compare the $H_p(10)$ and $H_p(0.07)$ relative responses for 4 mm and 4.3 mm thick PTFE disks of diameter 18 mm, for the 16 keV and 24 keV sources at 0° and -60° (horizontal) incidence, with a 20 keV source also considered for the latter filter.

Figures 8(a) and (b) show the $H_p(10)$ and $H_p(0.07)$ relative responses for just the 4.3 mm thick PTFE disk, at horizontal angles of 0°, -30° and -60°, for the entire ISO Narrow-Series and also ^{137}Cs, ^{60}Co, $^{12}C(p,p'\gamma)^{12}C$ and $^{19}F(p,\alpha\gamma)^{16}O$. As is evident, the 4.3 mm response is superior to that resulting from a 3.73 mm thick disk, as featured in Figures 6(a) and (b).

A TLD with a filter comprising a 4.3 mm thick PTFE disk of 18 mm diameter, covered by 2 mm PP, represents the final design arrived at in this study. It is seen to be a satisfactory dosemeter in respect of the given considerations, exhibiting acceptably flat and unitary relative response characteristics over the energy and angle range of interest. This final design is the configuration shown in Figures 1(a) - (c), and is the prime focus of the work described in the following sections, where its performance under various conditions is assessed.

[B] From the Continuous-Slowing-Down Approximation (*CSDA*) range data given in ICRU Report 37 [ICRU, 1984] for PP and PTFE. For PTFE, the surface density $\sigma^{(PTFE)}$, (= $t\times\rho$, for thickness t and density ρ) was used to read-off the maximum energy of electrons that can be stopped. Linearity was assumed between data points. The energy, X, lost in the PP was estimated from the quoted '*CSDA range*' value for E MeV electrons by using the relationship $X=(\sigma^{(PP)}\div[CSDA\ range])\times E$, which is valid for $\sigma^{(PP)}<[CSDA\ range]$. A reference initial energy of E=2 MeV was adopted.
For example, 2 mm PP has $\sigma^{(PP)}$=0.18 g/cm^2, which will 'slow' a 2 MeV electron by 0.377 MeV, whilst 4 mm PTFE has $\sigma^{(PTFE)}$=0.88 g/cm^2, which will stop a 1.55 MeV electron. The overall combination will therefore stop a 1.927 MeV electron.

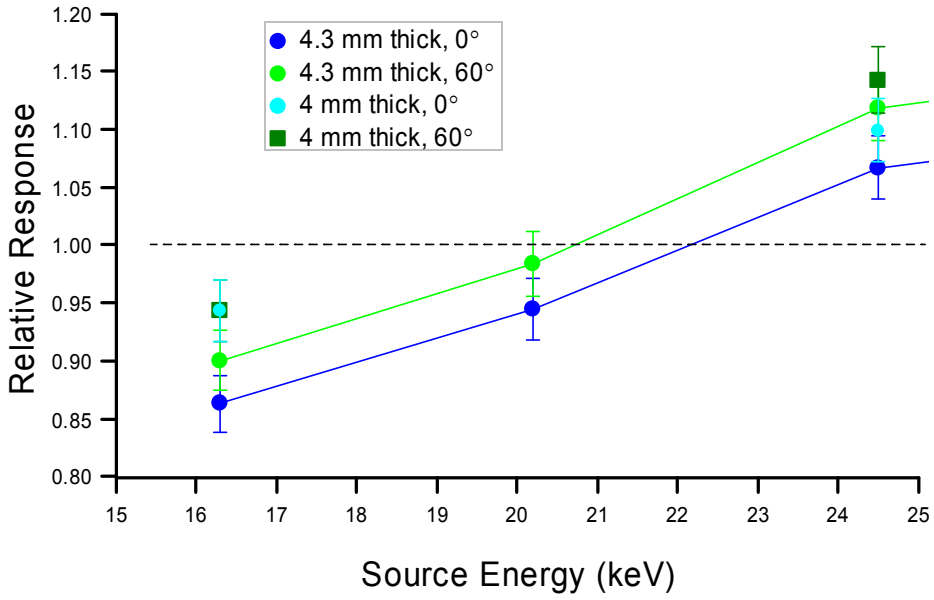

Figure 7(a): Comparison of the MCNP4c2-calculated $H_p(10)$ relative responses for TLD designs with 4 mm or 4.3 mm thick PTFE disks of diameter 18 mm, for low-energy sources at incidence angles of 0° and -60°.

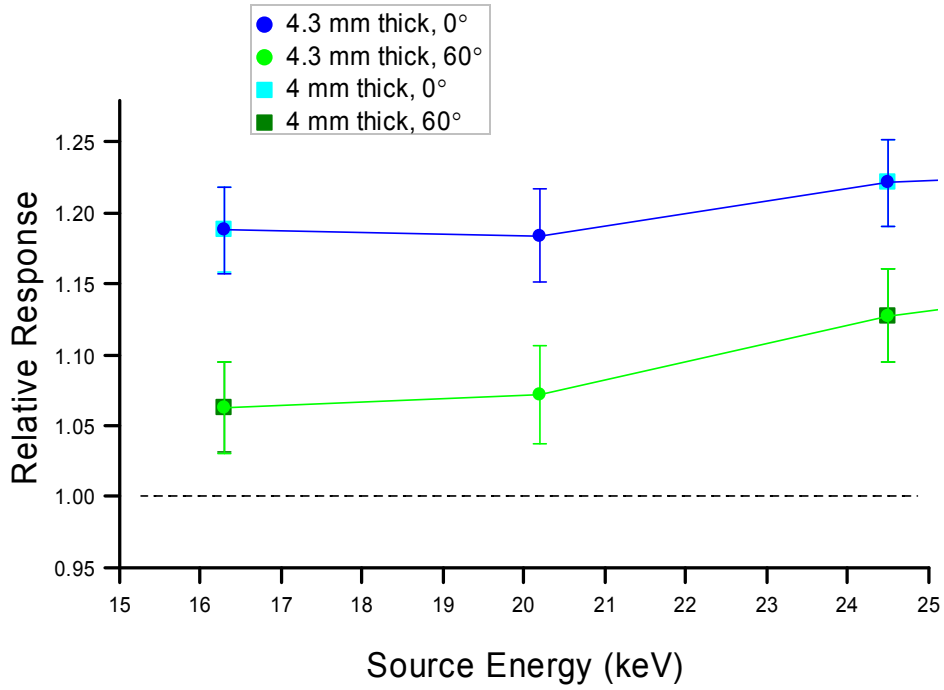

Figure 7(b): Comparison of the MCNP4c2-calculated $H_p(0.07)$ relative responses for TLD designs with 4 mm or 4.3 mm thick PTFE disks of diameter 18 mm, for low-energy sources at incidence angles of 0° and -60°.

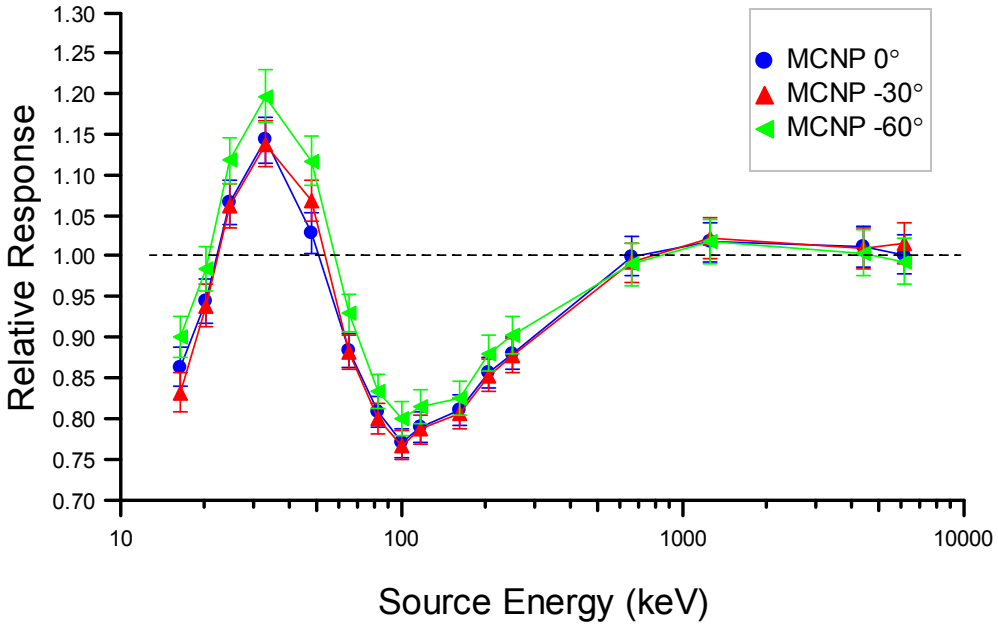

Figure 8(a): The MCNP4c2-calculated $H_p(10)$ relative responses of the final TLD design, incorporating a 18 mm diameter, 4.3 mm thick PTFE disk, at angles of 0°, -30° and -60°.

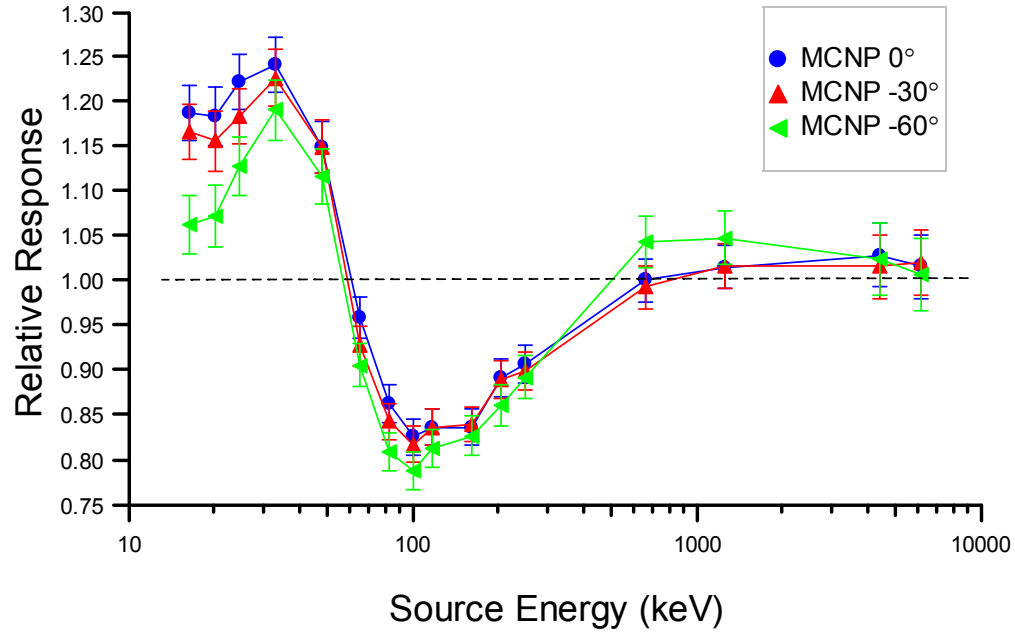

Figure 8(b): The MCNP4c2-calculated $H_p(0.07)$ relative responses of the final TLD design, incorporating a 18 mm diameter, 4.3 mm thick PTFE disk, at angles of 0°, -30° and -60°.

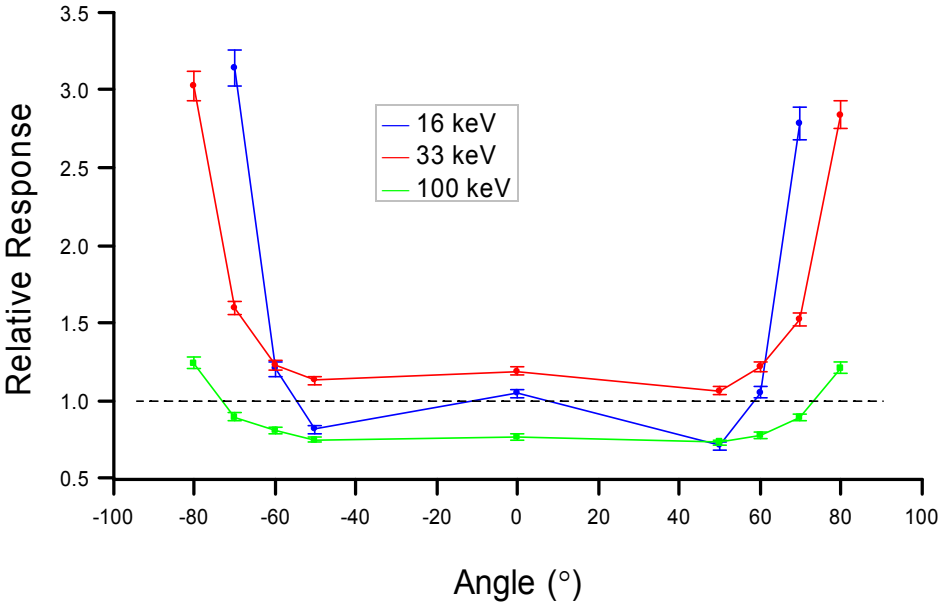

Figure 9(a): The MCNP4c2-calculated $H_p(10)$ relative responses of the final TLD design, incorporating a 4.3 mm thick, 18 mm diameter PTFE disk, for 16 keV, 33 keV and 100 keV sources at angles between -80° and +80°. Conversion coefficients taken from ISO 4037-3 were used.

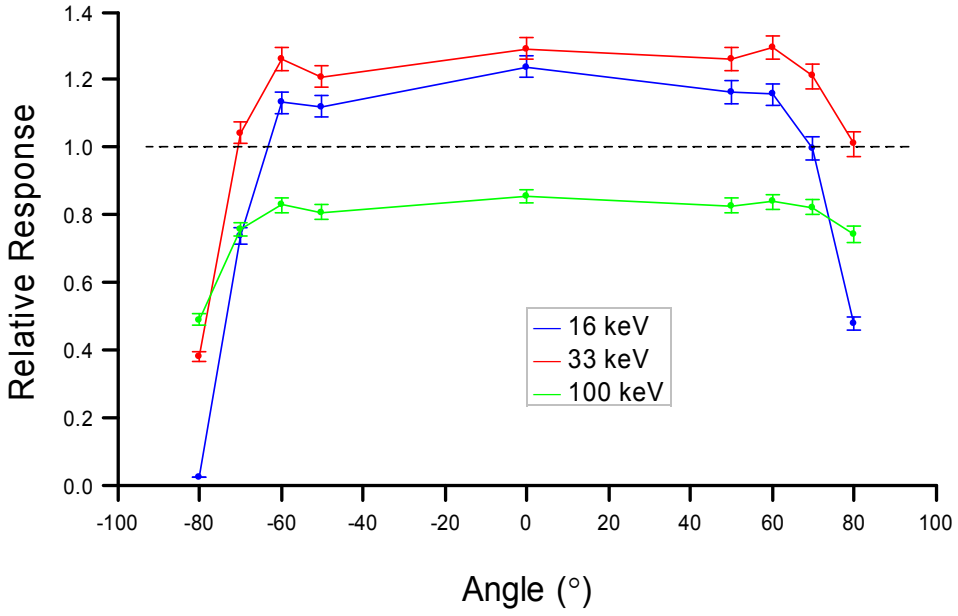

Figure 9(b): The MCNP4c2-calculated $H_p(0.07)$ relative responses of the final TLD design, incorporating a 4.3 mm thick, 18 mm diameter PTFE disk, for 16 keV, 33 keV and 100 keV sources at angles between -80° and +80°. Conversion coefficients taken from ISO 4037-3 were used.

7 ROTATIONAL IRRADIATION

With the final design of TLD established, its performance was evaluated relative to various sets of criteria. The first of these were its responses to sources incident at horizontal angles ranging from -80° to +80°.

The configuration was 'irradiated' in the model at angles in the horizontal plane of 0°, ±50°, ±60°, ±70° and ±80°; approximate constancy of response was assumed between 0° and ±50°. Along with Cs-137 (at 0°, for normalization), Narrow Series sources at three energies were considered: 33 keV, which corresponds to the maximum response of the TLD (Figures 8(a) and (b)); 100 keV, which corresponds to the minimum response of the TLD; and 16 keV, which is the lowest-energy field available at HPA. In this way, a reasonable overview of the performance of the dosemeter could be evaluated without repeating the simulations for the entire Narrow Series. Unlike previously, it was the conversion coefficients given in ISO 4037-3 [ISO, 1999] that were used for all $H_p(10)$ and $H_p(0.07)$ calculations; this was in part because PTB [Ankerhold, 2000] does not provide data for all of the angles of interest. The resulting $H_p(10)$ and $H_p(0.07)$ relative responses are shown in Figures 9(a) and 9(b).

As with the 10 mm diameter PTFE disk configuration discussed in Section 5, the $H_p(10)$ over-response at angles far from the normal is suggested to be a consequence of a high fraction of the detected photons entering the holder through the side rather than the front of the filter: the attenuation provided is hence not equivalent to a 10 mm thickness of tissue. As might be expected, the result of this effect was most significant at low energies, where the conversion coefficients are the most sensitive: the angle of incidence at which these effects become significant falls with decreasing photon energy (Figure 9 (a)).

A 'reverse' type of process appeared to be occurring with the $H_p(0.07)$ result (Figure 9(b)): between about 60°-70°, the $H_p(0.07)$ element is partially shadowed by the PP front-face of the TLD, and at more extreme angles it is likely that the photons were missing the hole completely on their way to the LiF element. An under-response consequently arose at high incidences. In other words, the suggestion is that the shape of the device leads to different levels of attenuation at different extreme angles due to the photons traversing different regions of the TLD structure. Careful consideration of the geometry of Figure 1(c) illustrates these points.

As seen from Figures 9(a) and 9(b), there exists an inherent asymmetry between the positive and negative angle responses. This phenomenon is conjectured to result from the inherent asymmetry of the device itself, as discussed below. The scale of the asymmetry may be estimated by comparing the average response at positive angles with the average response at negative angles. To this end, the average relative responses, $A_R(\alpha,\beta)$, in the angle domain from $\alpha°$ to $\beta°$ are given in Tables 3, 4 and 5, where the relative response was assumed to be constant between ±40°, which is supported by the data (Figures 9(a) and 9(b)). The results have standard uncertainties of a few percent. Note that the domain for the 16 keV source is confined to ±70° in the $H_p(10)$ case (Table 3), in order to avoid the worst of the over-response from causing a

misleadingly high answer. The bracketed letters **[A]** - **[F]** in Tables 3, 4, and 5 indicate the equation from which the values were derived. That is:

[A] $A_R(-70,70) = [\{R(-70)+R(-60)\}\div 2 + \{R(-60)+R(-50)\}\div 2 + \ldots + \{R(60)+R(70)\}\div 2] \div 14$

$= [\{R(-70)/2\} + R(-60) + R(-50) + \{9\times R(0)\} + R(50) + R(60) + \{R(70)/2\}]\div 14$

[B] $A_R(-70,0) = [\ \{R(-70)/2\} + R(-60) + R(-50) + \{9\times R(0)/2\}\ ] \div 7$

[C] $A_R(0,70) = [\ \{9\times R(0)/2\} + R(50) + R(60) + \{R(70)/2\}] \div 7$

[D] $A_R(-80,80) = [\ \{R(-80)/2\} + R(-70) + R(-60) + R(-50) + 9\times R(0) + R(50) + R(60) + R(70) + \{R(80)/2\}\ ] \div 16$

[E] $A_R(-80,0) = [\ \{R(-80)/2\} + R(-70) + R(-60) + R(-50) + \{9\times R(0)/2\}\ ] \div 8$

[F] $A_R(0,80) = [\ \{9\times R(0)/2\} + R(50) + R(60) + \mathrm{R}(70) + \{R(80)/2\}\ ] \div 8$

where $R(\theta)$ is the relative response at $\theta°$.

TABLE 3 $H_p(10)$ Average Relative Response in the stated angle domain.

Energy (keV)	$A_R(-70,70)$ [A]	$A_R(-70, 0)$ [B]	$A_R(0,70)$ [C]
16	1.16	1.19	1.12

TABLE 4 $H_p(10)$ Average Relative Response in the stated angle domain.

Energy (keV)	$A_R(-80,80)$ [D]	$A_R(-80, 0)$ [E]	$A_R(0,80)$ [F]
33	1.34	1.35	1.32
100	0.81	0.82	0.81

TABLE 5 $H_p(0.07)$ Average Relative Response in the stated angle domain.

Energy (keV)	$A_R(-80,80)$ [D]	$A_R(-80, 0)$ [E]	$A_R(0,80)$ [F]
16	1.11	1.07	1.14
33	1.22	1.19	1.26
100	0.82	0.81	0.84

As can be seen from the tables, negative angle $H_p(10)$ responses are greater than their positive angle counterparts, whereas the reverse is true for $H_p(0.07)$ responses. Corresponding asymmetries were also found in the type-test data [Gilvin *et al*, 2007]. By performing additional MCNP calculations, the most likely cause of this positive/negative asymmetry was shown to be differing contributions to the dose from photons scattered back from the phantom. This effect warranted a research programme in its own right [Eakins, 2006]; but, to provide a very simple schematic explanation, consider sources at horizontal angles of ±60°. For +60° sources, photons backscattered into the $H_p(10)$ element may have passed through the materials (PP, aluminium, etc.) contained within the '$H_p(0.07)$ side' of the TLD device on their path to the phantom, and as such are likely to have been attenuated. For -60° sources, however, photons backscattered into the

$H_p(10)$ detector are more likely to have impinged on the phantom directly, simply because this element is positioned towards the right edge of the holder (viewed from face-on). In other words, at +60° the 'shadow' created by the device is located directly behind the $H_p(10)$ element, whereas at -60° it is instead centred behind the $H_p(0.07)$ detector side of the dosemeter. At -60°, therefore, the backscattered contribution to the $H_p(10)$ dose can be greater, and consequently the overall response is increased. If the phantom were not present, the responses to +60° and -60° irradiation would be more equal.

Conversely, for the $H_p(0.07)$ response the opposite situation is true: because this element is positioned in the left side of the device, it is the doses from sources at positive angles that are greater. Backscatter, however, accounts for only a small fraction of the $H_p(0.07)$ response to 16 keV photons, so this asymmetry is not greatly apparent in Figure 9(b). Indeed, the large differences between the -80° and +80° $H_p(0.07)$ responses are more likely to be due to shadowing of the detector by the $H_p(10)$ filter, or other factors related to the physical structure of the device.

8 LATERAL IRRADIATION

In accordance with international guidelines [IEC, 2006], the 'lateral' response of the proposed final TLD design also needed to be evaluated, i.e. the response to horizontal exposures from the 'side'. This calculation was different from those featured previously: in particular, for a given source energy, it was the overall response averaged over a specified angle range that was required. Moreover, the quantity is defined in vacuum, i.e. with the phantom material 'voided'.

At a given energy, the average lateral response was calculated by evaluating the absorbed doses to the LiF at a succession of angles in the horizontal plane, normalizing each to the dose at 0°, and then calculating their mean. Angles increasing by increments of 10° were used. So overall, for a given set of equal-energy irradiations at angles $\theta=\alpha°,(\alpha+10)°,\ldots,\beta°$ that produced calculated per-source-particle doses of $D_{LiF}(\theta)$ in the LiF detector of interest (determined via an MCNP '*f6:p*' tally), the average lateral response $\overline{R}(\alpha,\beta)$ across the angle region of concern was given by

$$\overline{R}(\alpha,\beta)=\left(\frac{10}{10+\beta-\alpha}\right)\frac{\sum_{\theta=\alpha}^{\beta}D_{LiF}(\theta)}{D_{LiF}(0)}$$

The Cs-137 and 16 keV, 33 keV and 100 keV Narrow Series sources were considered, with these energies chosen on the same basis as for the calculations of Section 7, and both the $H_p(10)$ and $H_p(0.07)$ detectors tallied. For each source, two angle regions were evaluated: $60°\leq\theta\leq120°$ and $-120°\leq\theta\leq-60°$. The results are shown in Table 6.

TABLE 6 Lateral Response of final TLD design

	$\overline{R}(\alpha,\beta)$ for $H_p(10)$ detector		$\overline{R}(\alpha,\beta)$ for $H_p(0.07)$ detector	
Energy (keV)	**60° to 120°**	**-60° to -120°**	**60° to 120°**	**-60° to -120°**
16	1.23 (0.03)[(a)]	1.25 (0.03)	0.56 (0.01)	0.47 (0.01)
33	0.82 (0.01)	0.90 (0.02)	0.80 (0.02)	0.66 (0.02)
100	0.89 (0.02)	0.95 (0.02)	0.90 (0.02)	0.79 (0.02)
661.661	0.94 (0.02)	0.97 (0.02)	0.95 (0.02)	0.89 (0.02)

(a) One standard deviation statistical uncertainty

It is noted that the 16 keV, $H_p(10)$ detector results of 1.23 ± 0.03 (60° to 120°) and 1.25 ± 0.03 (-60° to -120°) lie just outside of the limit of 1.2 prescribed in the standard [IEC, 2006]. However, it is considered that the standard is not well formulated, in part because it is defined in the absence of a phantom yet includes irradiation at angles greater than 90° and is for dosemeters designed for on-body use, and in part because the scientific basis for choosing the value of 1.2 is arguably questionable. With this in mind, it is remarked that if the response at $(\theta+5)°$ were assumed to be the average of the responses at $\theta°$ and $(\theta+10)°$, then it can be shown that the 16 keV average lateral relative response of the $H_p(10)$ detector in the range from 65° to 115° is only 1.13 $\pm$ 0.02, whilst in the range from -65° to -115° it is 1.16 ± 0.03.

9 VERTICAL IRRADIATION

The response of the dosemeter to photons incident from vertical angles was also considered. Specifically, exposures were simulated from low-energy sources located above and in-front of the TLD, emitting plane-parallel photons that, in the laboratory frame-of-reference, had velocity vectors with components that were zero in directions parallel to the line joining the centres of the LiF elements. Sources that impinged on the device at angles of 30° and 60° to the reference normal (i.e. the perpendicular to the front-faces of the TLD and phantom) were modelled. Relative responses were calculated using Equation (1), with Ankerhold conversion coefficients used for $H_p(10)$. For $H_p(0.07)$, the Ankerhold conversion coefficients were used at 16 keV, with the values for 30° and 60° set the same as the 0° coefficient in each case; for 24 keV and 33 keV, ISO 4037-3 coefficients were employed, with $k(30,E) \neq k(60,E)$. For Cs-137, the Ankerhold $H_p(10)$ conversion coefficients were used for $H_p(0.07)$. The reasons for these choices are the same as those discussed in Section 2.3 for the horizontal exposures. The results are shown in Figures 10(a) and 10(b), with the low-energy responses for -30° and -60° horizontal exposures also provided for comparison.

As stated, the vertical exposures considered here correspond to sources incident from above. However, a symmetry of results could actually reliably be assumed for low or intermediate angle exposures from either above or below, due the effective up / down symmetry of the device (i.e. about a horizontal plane through the centres of the LiF elements) for low and intermediate angles, as seen in Figures 1(a)-(c). But, such an assumption could not be made at high angles (i.e. around 90°), where the intrinsic

asymmetry of the configuration would ultimately become significant. In such cases, photons would generally pass through more material when originating from a source located above the dosemeter than from a source positioned below, because the TL elements are located in the lower positions of the Harshaw card (Figure 1(a)).

10 ELECTRON FILTRATION

Using data provided in range-energy tables [ICRU, 1984], the minimum energy of an electron able to penetrate to a depth of 10 mm in ICRU 4-element tissue[C] can be shown to be approximately 2 MeV. It can similarly be shown that a 2 MeV electron can be stopped by a filter consisting of at least 4.3 mm PTFE covered by 2 mm PP. This capability is an important factor in the TLD's design, in order for it to accurately determine $H_p(10)$ in radiation fields containing electrons, including non-equilibrium fields of high-energy photons.

It is beneficial to use MCNP to confirm the above estimates for the electron ranges, and thus investigate the quality of the electron filtration by the proposed TLD design. To this end, two analyses were performed: an investigation into electron attenuation by the filter (Section 10.1); and an investigation into the fluence-energy distribution emergent from the filter (Section 10.2). These calculations are summarized in turn below, with a fuller discussion presented elsewhere [Eakins *et al*, 2007a]. In each case, two simple MCNP geometries were considered:

i) A 300 x 300 x 10 mm^3 slab of ICRU 4-element tissue;

ii) A 300 x 300 mm^2 slab of PP of thickness 2 mm, the 'back' face of which was completely coincident with the 'front' face of a 300 x 300 mm^2 slab of PTFE of thickness 4.3 mm.

Both configurations were surrounded by vacuum. An electron 'pencil beam' of radius 1 mm was perpendicularly incident on the front face of each configuration, centred on its geometric mid-point.

10.1 Attenuation

An MCNP '*f2:e*' electron fluence tally was defined on a 100 mm radius disk located in the plane of the back face of each configuration, centred on its geometric mid-point. A similarly tallied region was also defined on the front face. Thus, incident and transmitted electron fluences could readily be compared. The simulations were run in full electron/photon transport mode, but, in order to tally only primary electron fluence, the relevant input parameters were modified so that secondary electron and photon creation events were disabled.

[C] Composed of 76.2 % oxygen, 11.1 % carbon, 10.1 % hydrogen and 2.6 % nitrogen by mass, and of unit density [ICRU, 1980].

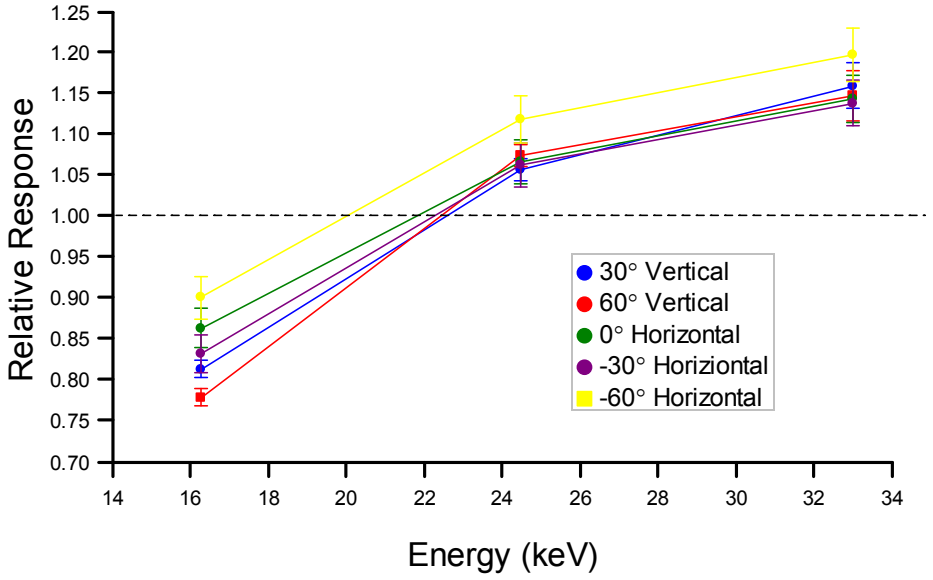

Figure 10(a): The MCNP4c2-calculated $H_p(10)$ relative responses of the final TLD design, incorporating a 4.3 mm thick, 18 mm diameter PTFE disk, for 16 keV, 24 keV and 33 keV sources incident at angles of 30° and 60° from above. Results from the previous horizontal exposures are also shown for comparison.

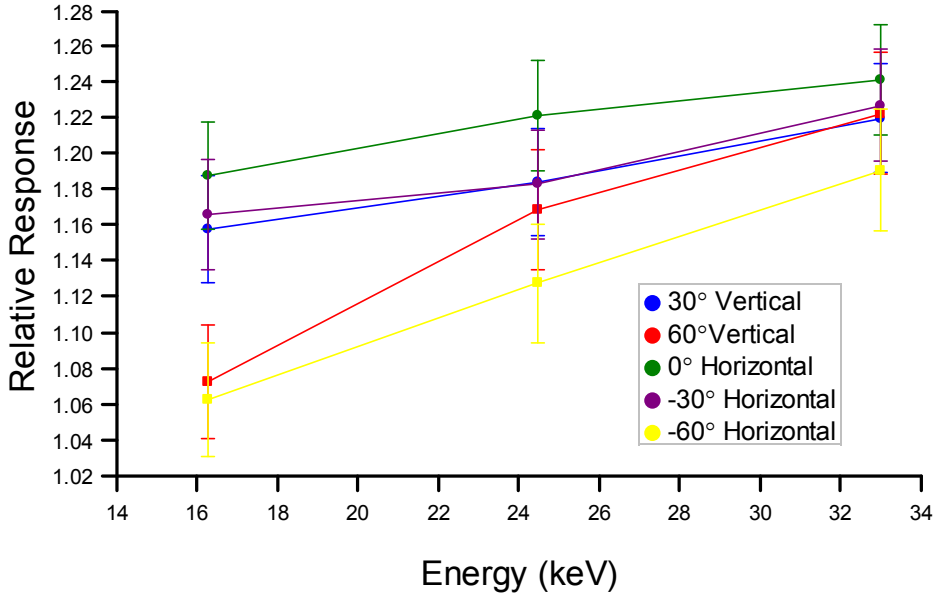

Figure 10(b): The MCNP4c2-calculated $H_p(0.07)$ relative responses of the final TLD design, incorporating a 4.3 mm thick, 18 mm diameter PTFE disk, for 16 keV, 24 keV and 33 keV sources incident at angles of 30° and 60° from above. Earlier results from horizontal exposures are shown for comparison.

The attenuation was calculated by normalizing the fluence of electrons emerging from the back of the configuration to the fluence incident on its front face. For the tissue configuration, the intensity of electrons emerging from the slab was found to drop off sharply below incident electron energies of about 2.25 MeV. Specifically, it was shown that 10 mm of ICRU 4-element tissue reduced the intensity of a source of 2.125 MeV electrons to about 2.5 % of incident fluence; to less than 0.3 % for a 2 MeV electron source; and to less than 0.01 % for 1.875 MeV electrons. The range in tissue of a 2 MeV electron was therefore confirmed as being approximately 10 mm, as expected.

For the PP+PTFE configuration with a 2 MeV electron source, the fluence of electrons emerging from the filter was similarly found to be approximately 0.3 % of the incident fluence. This compares well with the previous result for a 10 mm slab of tissue, and demonstrates the validity of the range/energy table-derived estimate that a 4.3 mm thick PTFE layer covered by 2 mm of PP is effectively equal to the range of 2 MeV electrons.

10.2 Fluence-Energy Distribution

The 'back' face *f2:e* tallies were energy-binned in order to gain insight into the distributions of the electron fields emerging from the configurations. Bins of width 0.1 MeV were used, with the data in each bin normalized to the incident fluence. For each configuration, two sets of calculations were performed:

a Calculations for which the secondary electron and photon creation events were again disabled;
b Calculations for which secondary electron and photon creation events were re-enabled, i.e. with the input parameters re-set such that MCNP ran in its default mode of operation for joint photon-electron problems.

The results are shown in Figure 11, for both the ICRU 4-element tissue and the PP+PTFE configurations. The datapoints on the graph are the relative fluence in each bin plotted at the bin's average energy.

As can be seen, the energy distribution of electrons transmitted through the PP+PTFE was similar to that emerging from the tissue. This agreement provided additional confirmation of the approximate equivalence of 4.3 mm PTFE covered by 2 mm PP to 10 mm tissue in terms of electron attenuation, and hence the suitability of the filter adopted. Moreover, it is argued that the similarities between the 'primary electron only' data (i.e. from '*a*') and the physically 'more real' results (i.e. from '*b*') indicate that the former are the outcome of a reliable method for determining the electron attenuation in the two configurations, and hence that the assumptions used in Section 10.1 to assess ranges in terms of primary-particle fluence reduction were appropriate for the purpose.

Finally, with secondary particle transport enabled, it is also possible to discuss the photon fields present at the tallying disk. Specifically, by defining an MCNP '*f2:p*' photon fluence tally on the surface-of-test of each configuration, it was found that the total fluence of photons emerging from the tissue slab differed from that from the PP+PTFE configuration by less than 10 %. This result again enforced the suggestion that 4.3 mm of PTFE covered by 2 mm of PP provides an appropriate substitute for 10 mm of tissue

for $H_p(10)$ assessments in mixed electron-photon fields, and hence further demonstrated the suitability of the PP+PTFE filter for use in the TLD. In both configurations, the photon fluence was higher than the analogous electron fluence by a factor of approximately 50.

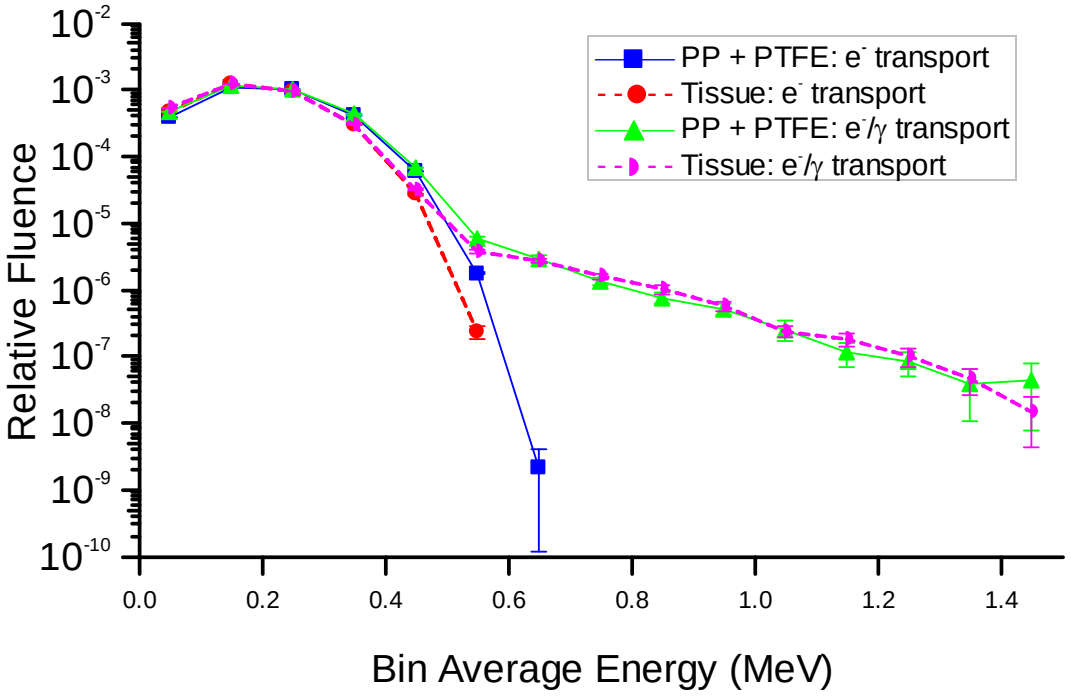

Figure 11: MCNP4c2-calculated energy distribution of electrons transmitted through: *i)* 4.3 mm PTFE covered by 2 mm PP; and *ii)* 10 mm of ICRU 4-element tissue. A monoenergetic 2 MeV source was used. The result in each bin is normalized to the incident electron fluence. Results are presented corresponding to both primary-electron-only, and full secondary electron/photon, transport calculations.

11 METHOD VALIDATION: CONVERSION COEFFICIENTS CALCULATION

As a final check on the validity of the MCNP methods used throughout this work, values for the air kerma to $H_p(10)$ conversion coefficients were calculated for selected energies within the range of interest, and compared against published data. These simulations involved just a single slab phantom of dimensions 300 × 300 × 150 mm^3, surrounded by vacuum in accordance with the kerma approximation. To estimate tissue dose, the phantom was constructed from ICRU four-element tissue [ICRU, 1980] of unit density. Doses were tallied in a *z*-axial cylinder of radius 10 mm and height 0.02 mm, with its

right-circular faces centred at (0, 0, 9.99) and (0, 0, 10.01), where the Cartesian co-ordinates are given in millimetres relative to an origin placed at the centre of the 300 × 300 mm^2 front face of the phantom. The phantom's front face was in the plane z=0. The location and dimensions of the tally-cylinder were such that it was assumed to provide a reasonable estimate of absorbed dose at a depth of 10 mm; for a photon source, the absorbed dose in ICRU tissue should be equal to dose equivalent.

Air kerma to $H_p(10)$ conversion coefficients, $k(\theta,E)$, at a given source energy and angle were evaluated from the ratio:

$$k(\theta,E)=\left(\frac{Tally\ dose\ in\ tissue\ at\ \theta^\circ}{Tally\ dose\ in\ air\ at\ 0^\circ}\right)=H_p(10)/K_a$$

where the MCNP-calculated tissue dose per-source-particle, $H_p(10)$, is a function of energy and angle. The air kerma data, K_a, used to determine $k(\theta,E)$ were calculated by repeating the simulations with the phantom material replaced by air. Air kerma is not angle dependent (though it is dependent on photon energy), so only one calculation was required for each energy. Exposures both to monoenergetic sources and the ISO Narrow Series distributions were considered.

11.1 PTB Sources

The PTB spectra with mean energies of 16 keV, 33 keV and 100 keV were used, together with a monoenergetic ^{137}Cs source. Sources incident at horizontal angles (θ) of 0°, ± 30° and ± 60° were considered. The resulting air kerma to $H_p(10)$ conversion coefficients that were calculated are presented in Tables 7(a) - (c), with comparisons made to the corresponding data of Ankerhold [Ankerhold, 2000].

TABLE 7(a) Air kerma to $H_p(10)$ Conversion coefficients at 0°

Energy (keV)	MCNP $k(\theta,E)$	Ankerhold $k(\theta,E)$
16	0.360 (0.003)[(a)]	0.333
33	1.266 (0.009)	1.21
100	1.801 (0.01)	1.8
662	1.215 (0.006)	1.21

(a) One standard deviation statistical uncertainty

TABLE 7(b) Air kerma to $H_p(10)$ Conversion coefficients at ±30°

Energy (keV)	-30° MCNP $k(\theta,E)$	+30° MCNP $k(\theta,E)$	Ankerhold $k(\theta,E)$
16	0.298 (0.006)[(a)]	0.304 (0.002)	0.286
33	1.193 (0.024)	1.202 (0.008)	1.15
100	1.741 (0.023)	1.754 (0.010)	1.75

(a) One standard deviation statistical uncertainty

TABLE 7(c) Air kerma to $H_p(10)$ Conversion coefficients at ±60°

Energy (keV)	-60° MCNP $k(\theta,E)$	+60° MCNP $k(\theta,E)$	Ankerhold $k(\theta,E)$
16	0.136 (0.005)[(a)]	0.135 (0.002)	0.123
33	0.935 (0.031)	0.923 (0.007)	0.883
100	1.510 (0.026)	1.506 (0.010)	1.51

(a) One standard deviation statistical uncertainty

11.2 Monoenergetic Sources

Monoenergetic sources of 15 keV, 20 keV, 30 keV, 100 keV and 600 keV were also used in the model to irradiate the configuration, but only at normal incidence. Differently from before, the air kerma results were this time determined by replacing the material of the tallying region with air of density 0.00120484 g/cm^3 and mass composition: 75.5267 % nitrogen, 23.1781 % oxygen, 1.2827 % argon and 0.0124 % carbon, as per the ICRU specification, and substituting the remaining phantom material with vacuum. However, such a change was considered minor: for example, a re-adjustment in air density from 0.00120484 g/cm^3 to 0.0011974 g/cm^3 (as used in Section 11.1 and throughout this work, and also by Ankerhold) can be shown to leave the 15 keV results invariant to a precision level greater than 0.0001 %, which is well within the quoted statistical uncertainty.

Using the formula given earlier, the resulting absorbed doses per air kerma were calculated, and the values compared with the corresponding data given in Table A.24 of ICRU Report 57 [ICRU, 1998] and approximated in Table 27 of ISO 4037-3 [ISO, 1999]. The results are shown in Table 8.

TABLE 8 Air kerma to $H_p(10)$ Conversion coefficients at 0°

Energy (keV)	MCNP	ICRU Report 57
15	0.282 (0.002)[(a)]	0.264
20	0.644 (0.004)	0.611
30	1.159 (0.009)	1.112
100	1.814 (0.010)	1.811
600	1.228 (0.006)	1.226

(a) One standard deviation statistical uncertainty

The agreement between calculated results and published data in Tables 7(a-c) and 8 was taken to increase confidence in some of the MCNP methods and procedures used in the work discussed throughout this report.

12 EXPERIMENTAL TYPE-TESTING

With the final design of TLD agreed, prototyping began so that the performance of the dosemeter could be determined experimentally. The full details of this last stage in the dosemeter's development are discussed at length elsewhere [Gilvin *et al*, 2007]. The most important results, however, are reproduced in Figure 12, which correspond to the $H_p(10)$ and $H_p(0.07)$ relative responses for normal incidence (0°) exposures. As can be seen from a comparison with MCNP data (Figures 8(a) and 8(b), and repeated here) acceptable agreement was found between calculated and measured results, though some discrepancies are apparent at the extremes of the energy scale.

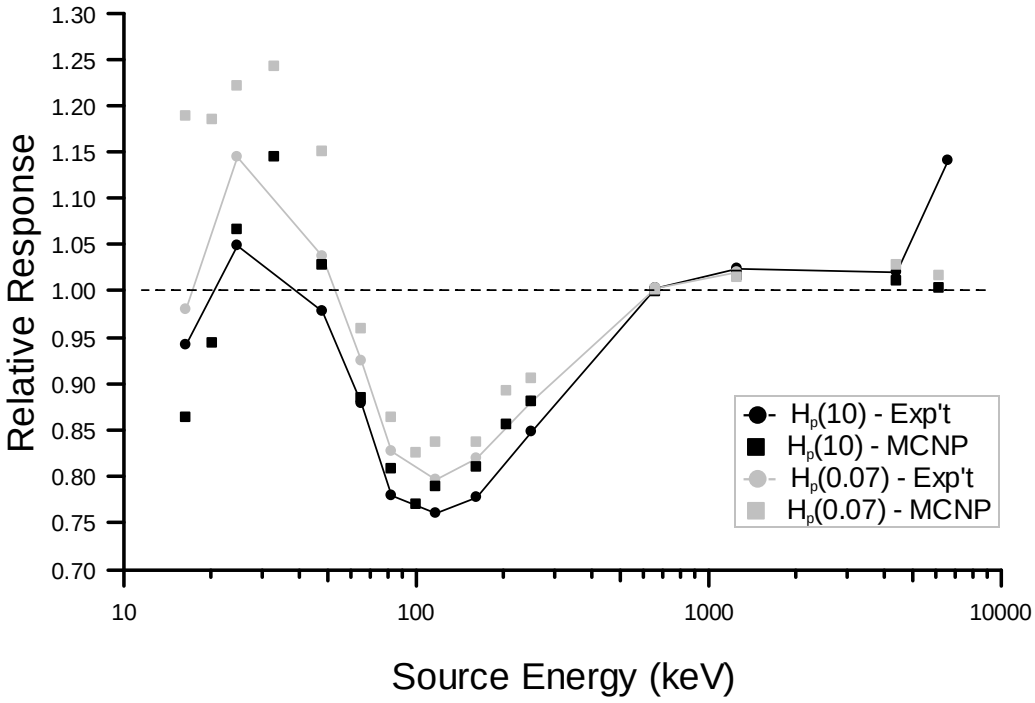

Figure 12: The measured $H_p(10)$ and $H_p(0.07)$ relative responses of the final TLD design for normal incidence exposures, incorporating an 18 mm diameter, 4.3 mm thick PTFE disk, corresponding to exposures at normal incidence. For comparison, the analogous MCNP4c2 calculated results are also shown.

13 MCNP4C2 VERSUS MCNP5

Shortly after the newly-designed TLD was rolled-out to issue by PDS, the updated Monte Carlo code MCNP5 [X-5, 2003] became available to users at HPA. MCNP5 is an improved version of its predecessor, MCNP4c2, containing, amongst other features, superior photoelectric effect cross section tables. This development raised the question of whether the MCNP code versions would give different results: specifically, would the

response characteristics that are calculated when MCNP5 is used be the same as those that were obtained previously using MCNP4c2? This issue is important, in part because research into the new TLD is considered on-going, not least due to continued interest in its performance in novel or unusual circumstances and fields that can only or best be assessed via Monte Carlo modelling. All future work will presumably be performed using the newest code available, but will also likely be compared against the MCNP4c2 data provided in this report and in the published papers [Eakins *et al*, 2007a; Eakins *et al*, 2007b]. An example of such post-design-stage work is the calculation of the ambient dose equivalent response of the TLD, discussed in the next section.

A full investigation into the differences between MCNP4c2 and MCNP5 has been conducted, and the consequences for the HPA TLD are described elsewhere [Eakins, 2008; Eakins 2009]. The main results are reproduced here. In summary, the $H_p(10)$ and $H_p(0.07)$ relative responses of the TLD to Cs-137 and the Narrow Series fields were recalculated for normal incidences using MCNP5, and compared against the analogous MCNP4c2 results illustrated in Figures 8(a) and 8(b). Figure 13 shows the ratio $[R(0,E)_{(5)}] \div [R(0,E)_{(4c2)}]$, where $R(0,E)_{(5)}$ is the relative response of the TLD to a source of mean energy E incident at 0° calculated using MCNP5, and $R(0,E)_{(4c2)}$ is the relative response of the TLD to a source of mean energy E incident at 0° calculated using MCNP4c2.

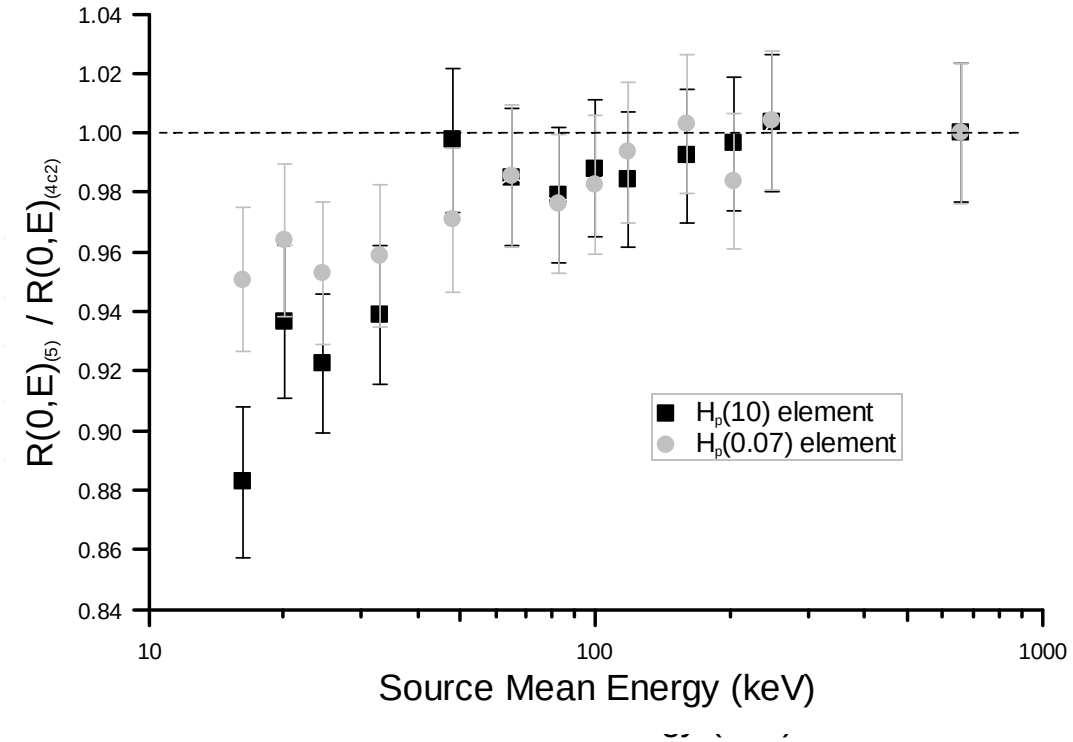

Figure 13: The ratios $[R(0,E)_{(5)}] \div [R(0,E)_{(4c2)}]$ between 10 keV and 1000 keV, where $R(0,E)_{(5)}$ is the relative response of the TLD calculated using MCNP5 for a photon source of mean energy E incident normally, and $R(0,E)_{(4c2)}$ is the analogous relative response calculated by MCNP4c2. The ratios for both the $H_p(10)$ and the $H_p(0.07)$ elements are shown.

One advantage of contrasting MCNP4c2 and MCNP5 responses by ratio is that the method removes the potential inclusion of any errors arising from the use of $\eta'(E)$ and $h(\theta,E)$, as might have occurred had responses calculated via Equation (1) been compared otherwise: recall that $\eta'(E)$ was determined using MCNP4c2 results. It is unclear what the best choices for $\eta'(E)$ or $h(\theta,E)$ will be in future response calculations using MCNP5. For instance, despite MCNP5 having access to superior cross section libraries, it may be that it would still be better to continue to use the older tables, or even the older MCNP4c2 code itself, and assume that any systematic uncertainties contained in $\eta'(E)$ are then effectively cancelled out. Alternatively, it might be preferable to determine a new, MCNP5-derived efficiency function, because the new cross section data are known to be an improvement over those that were included in the earlier version of MCNP. Similar issues exist surrounding the conversion coefficients, so simply changing the efficiency function could introduce systematic errors.

As can be seen from Figure 13, upgrading from MCNP4c2 to MCNP5 changed the response characteristics that were calculated for the new HPA TLD. The differences arose at low energies (< 100 keV), with differences of up to 10% occurring for energies less than ~50 keV. These discrepancies are as might have been predicted from considering the modifications to the photoelectric cross sections [Eakins 2008; Eakins 2009], an explanation further supported by the observation that the divergences diminished with increasing energy. Response data were not compared above 662 keV, but good agreement can be predicted from Figure 13 and from the knowledge that the cross sections for higher energies were not changed significantly.

The low-energy disparities will need to be considered in future TLD calculations, if results are to be compared with previous data. Moreover, it is quite possible that had MCNP5 been available to HPA during the latter stages of the design project, the final, optimized specifications of the TLD might have been subtly different. In particular, from a consideration of Figures 8(a) and 13 and the discussions of Section 6, it is conceivable that using MCNP5 might have lead to the adoption of a slightly thinner filter; from Figure 12 it can in turn be speculated that the subsequently measured $H_p(10)$ responses might then have been poorer at 24 keV, but improved at 16 keV and from 48 keV to 248 keV, and therefore the performance of the TLD might perhaps have been better overall. It is emphasized, however, that satisfactory performance was nevertheless demonstrated during extensive type-testing of the new design of dosemeter [Gilvin *et al*, 2007], as reported in Section 12.

14 *H**(10) RESPONSE

A customer of PDS expressed an interest in the ambient dose equivalent response characteristics that might be expected from the new HPA TLD. To investigate these, MCNP5 was used to model the device free in *vacuo* (i.e. in the absence of a phantom), irradiated by monoenergetic photon sources emitted isotropically inwards from the surface of a sphere 3.5 cm in radius. The centre of the sphere was coincident with the centre of the back face of the dosemeter. Sources at selected energies between 15 keV

and 300 keV were considered, as well as Cs-137. It was assumed that in the absence of the dosemeter, the field within the sphere would have been isotropic and homogenous.

The relative $H^*(10)$ response, $R^*(E)$, of the dosemeter to a source of energy E is defined as

$$R^*(E) = \left[\frac{D(E) \times h^*(Cs)}{D(Cs) \times h^*(E)} \right] \times \frac{\eta(E)}{\eta(Cs)}$$

where: $D(E)$ is the absorbed dose per-source-particle in the detector of interest (i.e. the $H_p(10)$ element or the $H_p(0.07)$ element), estimated here via an MCNP '*f6:p*' track-length tally; $h^*(E)$ is the fluence to ambient-dose-equivalent conversion coefficient at energy E; and $\eta(E)$ is the thermoluminescence efficiency of the LiF:Mg,Cu,P at E. The conversion coefficients, $h^*(E)$, at energies of 300 keV and below were taken from Table A.21 of ICRU 57 [ICRU, 1998]. For caesium-137, a value for $h^*(662)$ of 3.74 pSv cm^2 was used, obtained via a Lagrangian 4-point log-log interpolation of the ICRU 57 data at the 'closest' available energies, i.e. 500 keV, 600 keV, 800 keV and 1000 keV.

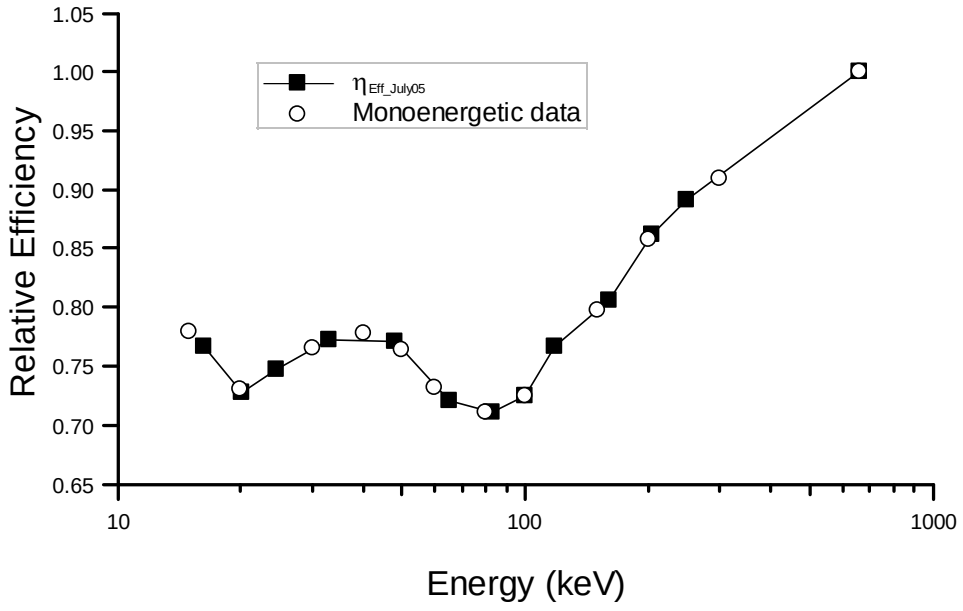

Figure 14: The MCNP4c2-derived efficiency function, $\eta_{Eff\text{-}July05}$, corresponding to Narrow Series sources (and Cs-137), and the efficiency data subsequently used for monoenergetic exposures in the MCNP5 calculations of the $H^*(10)$ relative response. Apart from the 15 keV value, which was extrapolated, the latter efficiencies were determined from the $\eta_{Eff\text{-}July05}$ dataset by interpolation.

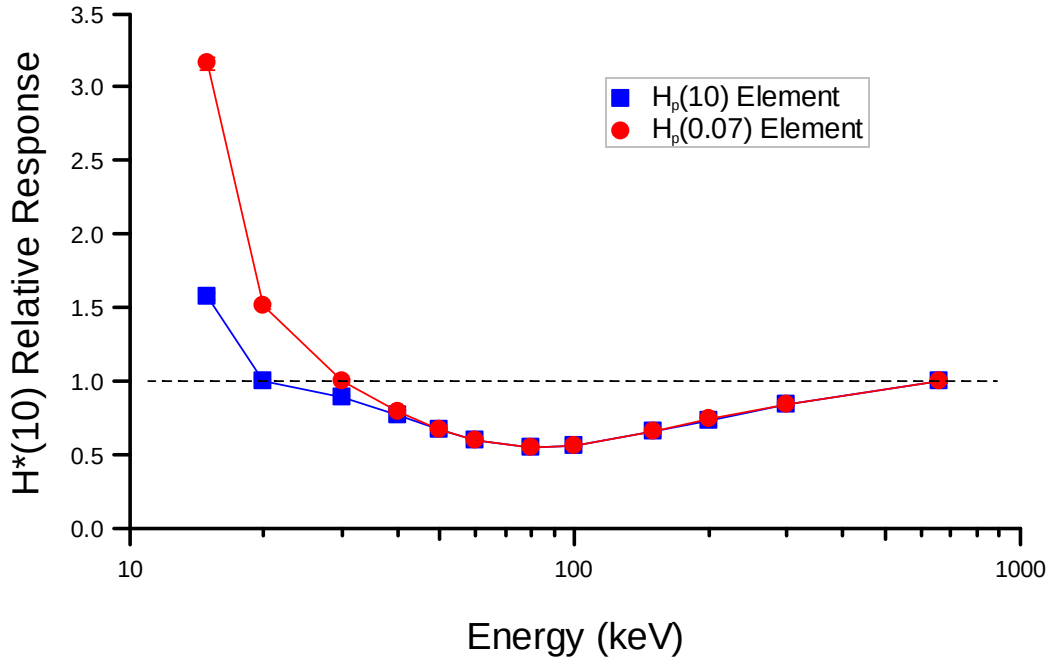

Figure 15: The *H(10) relative responses of both the $H_p(10)$ and $H_p(0.07)$ detector elements of the final TLD design, incorporating a 18 mm diameter, 4.3 mm thick PTFE disk, determined using MCNP5 and efficiency function data derived from $\eta_{Eff\text{-}July05}$. Isotropic, monoenergetic sources were used to expose the TLD, which was defined free-in-*vacuo*.**

Values for the efficiency function, $\eta(E)$, were obtained from the $\eta_{Eff\text{-}July05}$ data, which were derived previously by comparing MCNP4c2 results with measurements as described in Sections 3 and 4. As discussed in Section 13, it is unclear how accurate these data might be for MCNP5 analyses: they may, for example, contain systematic uncertainties that are cancelled out when they are used with MCNP4c2 calculations but not with MCNP5; future work programmes may involve reassessing the efficiency function using MCNP5. As seen in Table 2, the only data available below Cs-137 in the $\eta_{Eff\text{-}July05}$ set are for the ISO Narrow Series fields, which have mean energies between 16 keV and 248 keV (inclusive). For the monoenergetic sources between 30 keV and 200 keV (inclusive) considered now, the appropriate values for $\eta(E)$ were determined via Lagrangian 4-point log-log interpolations of the $\eta_{Eff\text{-}July05}$ data. For 15 keV, 20 keV and 300 keV, where insufficient data are available 'either side' to perform such a procedure, the efficiency values were estimated from a plot of $\eta_{Eff\text{-}July05}$ versus energy, either by direct interpolation (20 keV and 300 keV) or extrapolation (15 keV). The resulting values for $\eta(E)$ are shown in Figure 14 along with the $\eta_{Eff\text{-}July05}$ data, and given explicitly in Table 9. Confidence in the monoenergetic data is generally justifiable from Figure 14, though the extrapolation that was required to obtain the 15 keV datapoint implies that this individual result should perhaps be treated with some caution.

TABLE 9 Monoenergetic efficiency function, derived from $\eta_{Eff\text{-}July05}$ data.

Energy, *E* (keV)	**15**	**20**	**30**	**40**	**50**	**60**
Efficiency, $\eta(E)$	0.78	0.73	0.766	0.778	0.764	0.732
Energy, *E* (keV)	**80**	**100**	**150**	**200**	**300**	
Efficiency, $\eta(E)$	0.711	0.725	0.798	0.857	0.91	

The calculated $H^*(10)$ relative responses of the new TLD design are given in Figure 15, for both the $H_p(10)$ and the $H_p(0.07)$ elements of the dosemeter. It is seen that the $H_p(0.07)$ element over-responds significantly for lower photon energies, which is not unexpected, because it lacks the necessary filtration to simulate a depth of 10 mm. Similarly, the $H_p(10)$ element overestimates $H^*(10)$ at the lowest energies, because photons can reach the detector through the back of the badge without passing through the equivalent of 10 mm of tissue.

15 SUMMARY AND CONCLUSIONS

The overall aim of this work was to develop a personal photon/electron dosemeter according to a set of constraints, some chosen subjectively, others unavoidable. Specifically, the Monte Carlo code MCNP4c2 was used to design a holder for a TLD device containing LiF:Mg,Cu,P elements in a Harshaw TLD-700H card. The conclusion from the modelling project was that, out of all the candidates considered, the best performing configuration was the one shown in Figures 1(a) to 1(c). Such a dosemeter features a hole in front of the $H_p(0.07)$ detector, and a 4.3 mm thick, 18 mm diameter PTFE disk covered by 2 mm of polypropylene in front of the $H_p(10)$ detector. This PP + PTFE arrangement acts as an attenuating filter that acceptably approximates 10 mm of tissue, as required for accurate determination of the depth dose. The filtration is appropriate to both photon and electron fields; its suitability for the latter is demonstrated and discussed in Section 10.

Generally, the calculations were performed using MCNP4c2 in photon-only transport mode, with the kerma approximation applied. The resulting $H_p(10)$ and $H_p(0.07)$ relative responses of the dosemeter are shown in Figures 8(a) and 8(b) respectively, corresponding to simulated exposures to the full ISO Narrow Series spectra provided by PTB, and ^{137}Cs, ^{60}Co, ^{12}C(p,$p'\gamma$)^{12}C and ^{19}F(p,$\alpha\gamma$)^{16}O sources, at horizontal angles of 0°, -30° and -60° (i.e. impinging from the right in horizontal planes, as viewed from face-on). The rotational relative responses of the $H_p(10)$ and $H_p(0.07)$ detectors for 16 keV, 33 keV and 100 keV sources at angles from -80° to +80° are shown in Figures 9(a) and 9(b), respectively. The low-energy responses to sources at angles of 30° and 60° vertically above and in-front of the dosemeter are shown in Figures 10(a) and 10(b). The average lateral responses of the $H_p(10)$ detector in the angle ranges $60° \le \theta \le 120°$ and $-120° \le \theta \le -60°$ for 16 keV, 33 keV, 100 keV and 662 keV sources are shown in Table 6, and were almost all within the limit of 1.2 required by the relevant standard [IEC, 2006].

The $H^*(10)$ responses of the device in isotropic, monoenergetic fields are shown in Figure 15. Unlike the personal dose equivalent results, these data were calculated using the newer code MCNP5. Note that discrepancies of up to ~10 % can occur between MCNP4c2 and MCNP5 results in the photoelectric effect-dominated, low-energy region, as reported in Section 13 and elsewhere [Eakins 2008; Eakins 2009]. The $\eta_{Eff\text{-}July05}$ data were used in these calculations to derive values for the thermoluminescence efficiency of the LiF:Mg,Cu,P for monoenergetic sources; potential problems associated with this were discussed.

Type-test results obtained from measurements on the final design of TLD are shown in Figure 12. Encouragingly, acceptable agreement with the Monte Carlo estimates was shown. Of course, the experimental results should be considered the 'definitive' performance data for the new dosemeter [Gilvin *et al*, 2007].

This report represents an overview of work completed on the new HPA TLD, with the filter and configuration described above (Figures 1(a) to 1(c)) corresponding to its final design. Future endeavours may involve the use of MCNP5 in its physically more-realistic electron / photon mode, which allows electrons to be transported in addition to photons, and can hence fully investigate the performance of the device in mixed fields as well as determine improved estimates for the thermoluminescence efficiency function. Studies may also begin by evaluating all of the relevant conversion coefficients that are missing from the tabulations published by ICRU and ICRP, to ensure that the limited scope of these data does not impact on the responses calculated for the TLD. In time, such work could potentially lead to subsequent redesigns of the dosemeter.

16 ACKNOWLEDGEMENTS

The author would like to credit David Bartlett, formerly of HPA, and Luke Hager, Phil Gilvin and Rick Tanner, of HPA, for essential input, suggestions and discussions throughout the life-cycle of the project. The contributions by César Molinos-Solsona during his time at NRPB/HPA are also duly recognized. Jan Jansen is additionally acknowledged, for discussions on the issues surrounding MCNP4c2 versus MCNP5. Special thanks also to Ulrike Ankerhold of PTB for helpful correspondence and advice, and for supplying the data ultimately used as source distributions in many of the MCNP simulations. The irradiations up to 1253 keV were performed by the Metrology Group at HPA, and the R-C and R-F irradiations by Rolf Behrens at PTB.

17 REFERENCES

Alberts W G, Böhm J, Kramer H M, Iles W J, McDonald J, Schwartz R B and Thompson I M G (1994). International standardization of reference radiations and calibration procedures for radiation protection instruments, ISSN 1013-4506.

Ankerhold U (2000). Catalogue of X-ray spectra and their characteristic data-ISO and DIN radiation qualities, therapy and diagnostic radiation qualities, unfiltered X-ray spectra. PTB-Dos-34, PTB: Braunschweig.

Briesmeister J F (Ed) (2000). MCNP – a general Monte Carlo n-particle transport code, Version 4C. Report No. LA-13709-M. Los Alamos, LANL.

Casbolt P N, Marshall T O and Shaw K B (1973). A thermoluminescent personal dosemeter compatible with automatic processing and the central recording of dose histories. NRPB Report, UK.

Eakins J S (2006). MCNP and the design of the new HPA TLD Device - Part II: Calculating the effects of phantom backscatter, NRPB Tech. Memo [Unpublished].

Eakins J S, Bartlett D T, Hager L G, Molinos-Solsona C and Tanner R J. (2007a). The MCNP4c2 design of a two element photon/electron dosemeter that uses magnesium/copper/phosphorus doped lithium fluoride. Radiat. Prot. Dosim. 128(1), 21-35.

Eakins J S, Bartlett D T, Hager L G and Tanner R J (2007b). Monte Carlo modelling of a TLD device containing ^{7}LiF:Mg,Cu,P detectors. Radiat. Meas. 43(2), 631-635.

Eakins J S (2008). Photon cross section data in absorbed dose calculations. HPA Report HPA-RPD-049.

Eakins J S (2009). On the effect of updated MCNP photon cross section data on the simulated response of the HPA TLD. Radiat. Prot. Dosim. 134(1), 66-71 .

European Commission (1994). Radiation Protection 73: Technical recommendations for monitoring individuals occupationally exposed to external radiation. EC Report EUR-14852.

European Commission (2009). Radiation Protection 160: Technical recommendations for monitoring individuals occupationally exposed to external radiation. EC Contract TREN/07/NUCL/S07.70121.

Gilvin P J, Baker S T, Daniels T J, Eakins J S, McClure D R, Bartlett D T and Boucher C (2007). Type testing of a new TLD for the UK health protection agency. Radiat. Prot. Dosim. 128(1), 36-42.

Health and Safety Executive (2008). Requirements for the approval of dosimetry services under the ionising radiations regulations 1999; Part 1 - external radiations. HSE Report RADS1.

Hranitzky C, Stadtmann H and Olko P (2006). Determination of LiF:Mg,Ti and Li:Mg,Cu,P TL efficiency for x-rays and the application to Monte Carlo simulations of dosemeter response. Radiat. Prot. Dosim., 119 (1-4), 483-486.

International Commission on Radiological Protection (1997). General principles for the radiation protection of workers. ICRP Publication 75. Pergamon Press, Elsevier Science

International Commission on Radiation Units and Measurements (1980). Radiation quantities and units. ICRU Report 33. Washington DC, USA. ICRU.

International Commission on Radiation Units and Measurements (1984). Stopping powers for electrons and positrons. ICRU Report 37. Bethesda, USA. ICRU.

International Commission on Radiation Units and Measurements (1998). Conversion coefficients for use in radiological protection against external radiation. ICRU Report 57. Bethesda, USA. ICRU. *Jointly published as*: International Commission on Radiological Protection (1996), ICRP Publication 74. Pergamon Press, Elsevier Science.

International Electrotechnical Commission (2006). Thermoluminescence dosimetry systems for personal and environmental monitoring. IEC 61066:2006. Geneva IEC.

International Electrotechnical Commission (2007). Radiation protection instrumentation- Passive integrating dosimetry systems for environmental and personal monitoring; Part 1 – General characteristics and performance requirements. IEC 62387-1. Geneva IEC.

International Organization for Standardization (1989). Neutron reference radiations for calibrating neutron measuring devices used for radiation protection purposes and for determining their responses as a function of neutron energy. ISO 8529. Geneva, ISO.

International Organization for Standardization (1996). X and gamma reference radiation for calibrating dosemeters and doserate meters and for determining their response as a function of photon energy – Part 1: Radiation characteristics and production methods. BS ISO 4037-1.

International Organization for Standardization (1999). X and gamma reference radiation for calibrating dosemeters and doserate meters and for determining their response as a function of photon energy – Part 3: Calibration of area and personal dosemeters and the measurement of their response as a function of energy and angle of incidence. BS ISO 4037-3.

Kramer H M, Böhm J, Iles W J, and Thompson I M G (1994). On the current status of an ISO working document on the calibration and type testing of radiation protection dosemeters for photons. Radiation Protection Dosimetry **54** (3/4), 267-272.

McKinlay A F (1981), Thermoluminescence Dosimetry, Adam Hilger Ltd. (IoP publishing), Bristol.

Molinos Solsona C, Tanner R J and Bartlett D T (2004). MCNP™ optimization and experimental validation of the design of the new TLD holder. Physical Dosimetry Department Technical Memorandum (Draft).

Olko P (1996). Microdosimetric Interpretation of Thermoluminescence Efficiency of LiF:Mg,Cu,P (MCP-N) Detectors for Weakly and Densely Ionizing Radiations. Radiation Protection Dosimetry, **65**, 1-15.

Olko P, Bilski P, Budzanowski M, Waligórski M P R, Fasso A, and Ipe I (1999), Modelling of the thermoluminescence response of LiF:Mg,Cu,P (MCP-N) detectors after doses of low-energy photons. Radiation Protection Dosimetry **84** (1-4), 103-107.

Shaw K B and Marshall T O (1977). Technical specification of the NRPB thermoluminescent dosemeter used for the measurement of body dose and skin dose. NRPB.

X-5 Monte Carlo Team (2003). MCNP - A general Monte Carlo N-Particle transport code, Version 5. LANL Report LA-UR-03-1987.

APPENDIX A

Change Log

Being limited by the fixed dimensions of the TLD-700H card, as well as other requirements, the overall structure of the card / holder / phantom configuration was generally much the same throughout the design process. In particular, different potential designs were often only characterized by small differences in their specifications. As a result, to save time and minimize the possibility of introducing typing errors, the same 'core' MCNP input file was often used from one simulation to the next, with just relevant parameters modified as required. Most of these changes were made in order to study the effects of varying certain features, as described in this report, and hence some were only temporary.

However, permanent changes were also made. Some of these were significant, and effectively represented the convergence of the development project onto the final design; an example here would be the adoption of the 4.3 mm thick PTFE filter. Others, however, were considered relatively insignificant, and arose as decisions were made during the design process regarding the final appearance of the device or new information came to light; an example here would be a minor alteration in the width of the label-viewing window. Inconsequential modifications such as these are not mentioned in the main text of this document, partly because it was felt that doing so could detract from the accounts of the more significant alterations being made, changes in the filter thickness being an obvious example. Nevertheless, it is important to record them, not only for posterity, but also to pre-empt any discussion of their contributions, however small, to the changes in the performance of the device.

This appendix consequently serves as a brief 'event log' of these minor changes. It follows the same chronology as the main sections of the report, and therefore highlights the changes made in the core input file as the investigation proceeded from the set of trials described in one section to those of the next. The 'evolution' of the input file from a basic configuration resembling the old NRPB holder, to a version that defines the proposed final design, is thus seen.

A1 SECTION 3

The initial input file described the Harshaw TLD-700H card inside a variation of the 'old' holder design [Casbolt, 1973] that had its PP dome sheared to a 2 mm thickness. Because the old holder was designed to encompass the 'old' NRPB card, which was supplied by Vinten Ltd and is different in shape from the TLD-700H, the $H_p(0.07)$ hole in the holder front was not located directly over the corresponding LiF element. However,

since the $H_p(0.07)$ response was not considered in the calculations of Section 3, such a feature was not a problem.

A2 SECTION 4

The holder was redesigned significantly to account for the dimensions of the new Harshaw card. It became smaller, fitting the card exactly around the edges with no air gaps, and the skin-dose hole was located directly over the appropriate LiF element so that the $H_p(0.07)$ response could be evaluated. This configuration is referred to as the 'new design' in the following, even though it was still altered a number of times.

With the new design defined, the input file was actually changed again temporarily in Section 4. As described in the text of that section, the front of the holder was set as a solid PP block, and the holder depth was increased to permit the inclusion of the PTFE slab.

A3 SECTION 5

The 'new design' of Section 4 was adopted, with the filter and its covering defined as required. The circular face of the PTFE disk closest to the LiF element was positioned in the same plane as the back face of the PP that comprised the front of the holder. Tallies were defined on both LiF cells. Negative angle sources were used for the first time in Section 5, requiring the definition of a new set of MCNP surfaces. As a consequence, and for convenience, an additional file was written containing a 'uniform' set of surface and *sdef* cards, which could then be copied / pasted from when needed.

A4 SECTION 7

The holder was enlarged slightly in both height and width, in accordance with the dimensions expected of the final device; the likely presence of approximately 5 mm of crimping on the edges of the wrapping, for instance, necessitated a slightly wider internal size. The viewing window was also re-sized and re-positioned a little, to the optimum for label-reading in the final product. The PTFE filter was specified as being exactly 18 mm in diameter; this contrasted with the value of 17.92 mm used in Sections 5 and 6, which was previously only referred to as 18 mm. A 'universal' set of source surface cards was included; only the *sdef* card then needed to be modified each time in order to refer to whichever member of this set was required for the particular simulation of interest.

A5 SECTION 8

The hole in front of the $H_p(0.07)$ detector was redesigned. The hole was originally frustum shaped, with a minimum diameter of 11.1 mm and a maximum diameter of 13.4 mm, which resulted in side walls that were at angles of 30° to the frustum's central

axis. The redesigned hole was still a frustum, but was given the respective specifications: 12 mm and 15 mm (and hence 36.9°).

After Section 8, no further minor changes were made to the ‘core’ input file that specified the TLD.

APPENDIX B

MCNP Input File for Air Kerma Determination

The input file given below is that used to determine the dose in air at 16 keV. The file defines a configuration that represented an early trial in the design of the dosemeter, i.e. one that would have featured an aluminium filter, but with all materials changed to air. Despite being related to an obsolete design, however, the results from this simulation were used in all subsequent response calculations that required air kerma data at 16 keV; no problems were anticipated associated with this re-use. Similar files exist corresponding to the other Narrow Series spectra and monoenergetic sources.

```
MCNP input for Air Kerma Evaluation
c Cell cards...
c Card:
    1     3  -0.00120484 -1 $  Thick LiF
    2     3  -0.00120484 -2 $  Thin LiF
    3     3  -0.00120484 1 -3 $ Thick Teflon Cover
    4     3  -0.00120484 2 -4 $ Thin Teflon Cover
    5     3  -0.00120484 3 4 -5 -16 $ Teflon Sheet
    6     3  -0.00120484 -6 3 5 $ Air Front Thick
    7     3  -0.00120484 -7 4 5 $ Air Front Thin
    8     3  -0.00120484 -8 5 $ Air Front Right
    9     3  -0.00120484 -9 5 $ Air Front Left
   10     3  -0.00120484 -10 3 5 $ Air Back Thick
   11     3  -0.00120484 -11 4 5 $ Air Back Thin
   12     3  -0.00120484 -12 5 $ Air Back Right
   13     3  -0.00120484 -13 5 $ Air Back Left
   14     3  -0.00120484 6 7 8 9 -14 -16 $ Aluminium Front
   15     3  -0.00120484 10 11 12 13 -15 -16 $ Aluminium Back
   16     3  -0.00120484 -5 16 $ Teflon Corner cutoff
   17     3  -0.00120484 -14 16 $ Aluminium Front Corner Cutoff
   18     3  -0.00120484 -15 16 $ Aluminium Back Corner Cutoff
c Wrapper:
   19     3  -0.00120484 5 14 15 -17 $ EVA Layer
   20     3  -0.00120484 17 -18 $ PET Layer
c Gaps:
   21     3  -0.00120484 18 -19 $ Air Jacket
c Holder:
   22     3  -0.00120484 19 -20 $ Holder back and sides
   23     3  -0.00120484 -21 $ Aluminium disk
```

```
   24     3  -0.00120484 21 -22 $ Air Cavity
   25     3  -0.00120484 22 24 -23 25 $ Front Face
   26     3  -0.00120484 -24 $ Air Window
   27     3  -0.00120484 -23 -25 $ Cone Cutout
   28     3  -0.00120484 -26 27 $ Cylindrical Front Lump
   29     3  -0.00120484 -27 -30 $ Spherical Cutout of Air Cylinder
c Phantom:
   30     3  -0.00120484 -28 $ Water Fill
   31     3  -0.00120484 28 -29 $ Perspex Box
c Environment:
   32     3  -0.00120484 26 27 -30 $ Remains of Air Cylinder
   33     0  20 23 30 29 35 -31 $ Air or Vacuum for Kerma Approx.
c  Variance:
   34     3  -0.00120484 30 -35 $ Air Column
   99     0  31

c Surface cards...
c For the LiF:
    1      rcc    1.28551    -0.7321    -0.3027       0        $ Thick LiF
                  0      0.038       0.18
    2      rcc   -1.28551    -0.7321    -0.2962       0        $ Thin LiF
                  0      0.025       0.18
c For the Teflon:
    3      rcc    1.28551    -0.7321    -0.3091       0        $ Thick Tef
                  0     0.0508     0.1864
    4      rcc   -1.28551    -0.7321    -0.3026       0        $ Thin Tef
                  0     0.0378     0.1864
    5      rpp   -2.17551    2.17551    -1.5621     1.5621  $ Teflon Sheet
                  -0.2901    -0.2773
c For the Front Air Cylinders:
    6      rcc    1.28551    -0.7321    -0.3612       0       0  $ Thick F
                     0.0711       0.5
    7      rcc   -1.28551    -0.7321    -0.3612       0       0  $ Thin F
                    0.0711        0.5
    8      rcc    1.28551     0.7321    -0.3612       0       0  $ Right F
                     0.0711       0.5
    9      rcc   -1.28551     0.7321    -0.3612       0       0  $ Left F
                    0.0711        0.5
c For the Back Air Cylinders:
   10      rcc    1.28551    -0.7321    -0.2773       0       0  $ Thick B
                     0.0711       0.5
   11      rcc   -1.28551    -0.7321    -0.2773       0       0  $ Thin B
                    0.0711        0.5
   12      rcc    1.28551     0.7321    -0.2773       0       0  $ Right B
                     0.0711       0.5
   13      rcc   -1.28551     0.7321    -0.2773       0       0  $ Left B
                    0.0711        0.5
c For the Aluminium:
```

```
   14      rpp   -2.17551    2.17551    -1.5621     1.5621    $ Front Al
                 -0.3612    -0.2901
   15      rpp   -2.17551    2.17551    -1.5621     1.5621    $ Front Al
                 -0.2773    -0.2062
c Corner Cut-off Plane:
   16        p          1         -1          0    3.23761
c For the Wrapper:
   17      rpp   -2.17931    2.17931    -1.5659     1.5659     $ EVA layer
                 -0.365    -0.2024
   18      rpp   -2.18171    2.18171    -1.5683     1.5683     $ PET layer
                 -0.3674   -0.2
c For the Air Gaps:
   19      rpp   -2.18171    2.97829      -1.96     1.96    $ Air Jacket
                 -0.4674   -0.2
c For the Holder:
   20      rpp   -2.38171    3.17829     -2.16      2.16  $ Back and Sides
                 -0.4674    0
c For the Filter:
   21      rcc    1.28551    -0.7321    -0.6674       0     0 $ Al disk
                  0.07      0.7475
   22      rcc    1.28551    -0.7321    -0.6674       0     0 $ Air filter
                  0.2       0.8375
c For the Front Face:
   23      rpp   -2.38171    3.17829      -2.16      2.16    $ Plastic front
                 -0.6674    -0.4674
   24      rpp   -1.60171    2.39829      0.705      1.62    $ Air Window
                 -0.6674    -0.4674
   25      k/z   -0.50949   -0.7321   0.493074  0.3333333    -1     $ Cone
   26      rcc    1.28551   -0.7321    -0.8824       0        0     $ Lump
                 0.215      1.125
   27      sph    1.28551   -0.7321   -26.1824     25.325 $ Sphere cutout
c For the Phantom:
   28      rpp  -13.60171   14.39829       -14       14       $ Water fill
                 0.25       14
   29      rpp  -14.60171   15.39829       -15       15       $ Box
                 0          15
c For the Surroundings:
   30      rcc    1.28551    -0.7321    -0.9174        0      $ Air Cylind
                  0       0.25        1.5
   31      rpp  -22.60171     23.39829      -23       23     -4      $ Air
                   15.1
c For the Source:
   32       pz    -1.1674 $ 0 Degrees (Sources disks centred on 0,0,0)
   33        p          1          0    1.73205    -2.3348 $ 30 Degrees
   34        p    1.73205          0          1    -2.3348 $ 60 Degrees
c Variance:
   35      rcc    1.28551    -0.7321      -1.17       0     0 $ Air Cylind
                  0.5        2.5
```

```
mode  p
c
c Materials Specs:
m1    3007.         -0.266167 $ LiF:Mg,Cu,P
      3006.         -8e-005 9000.         -0.728752 12000.         -0.002
      29000.        -4e-005 15000.        -0.003
m2    6000.         -0.240183 $ Teflon
      9000.         -0.759817
m3    6000.         -0.000124 $Air
      7000.         -0.755267 8000.        -0.231781 18000.      -0.012827
m4    14000.        -0.0025 $ Aluminium card
      29000.        -0.001 12000.          -0.025 26000.           -0.004
      25000.        -0.001 24000.          -0.0025 30000.          -0.001
      13000.        -0.963
m41   13000.        -0.995 $ Aluminium Disk
      29000.        -0.0005 26000.          -0.004 12000.          -0.0005
      25000.        -0.0005 14000.          -0.0025 22000.         -0.0003
      23000.        -0.0005 30000.          -0.0005
m5    6000.          0.33333 $ EVA
      1000.          0.55556 8000.           0.11111
m6    6000.          0.45455 $ PET
      1000.          0.36364 8000.           0.18182
m7    1000.         -0.143711 $ Polypropylene
      6000.         -0.856289
m8    1000.         -0.111894 $ Water
      8000.         -0.888106
m9    1000.         -0.080538 $ Perspex
      6000.         -0.599848 8000.         -0.319614
c
c Cell Importancies:
imp:p  128         1           64          1           16          $ 1, 5
       32          1           6r          16          1           $ 6, 15
       3r          16          2r          1           16          $ 16, 23
       1r          8           1           8           2r          $ 24, 29
       1           1r          8           1           8           $ 30, 34
       0           $ 99, 99
c
c Source Definition:
sdef POS=0 0 -1.1674 SUR=32 RAD=d1 VEC=0 0 1 DIR=1 PAR=2 ERG=d3
si1  22
si3  h 0.007 0.0072 0.0074 0.0076 0.0078 0.008 0.0082 0.0084 0.0086 0.0088 &
       0.009 0.0092 0.0094 0.0096 0.0098 0.01 0.0102 0.0104 0.0106 0.0108 &
       0.011 0.0112 0.0114 0.0116 0.0118 0.012 0.0122 0.0124 0.0126 0.0128 &
       0.013 0.0132 0.0134 0.0136 0.0138 0.014 0.0142 0.0144 0.0146 0.0148 &
       0.015 0.0152 0.0154 0.0156 0.0158 0.016 0.0162 0.0164 0.0166 0.0168 &
       0.017 0.0172 0.0174 0.0176 0.0178 0.018 0.0182 0.0184 0.0186 0.0188 &
       0.019 0.0192 0.0194 0.0196 0.0198 0.02 0.0202 0.0204 0.0206 0.0208 &
```

```
       0.021 0.0212 0.0214 0.0216 0.0218 0.022  $ ENERGY 16.3
c
sp3  d 0 0.58542 0.23504 0.44782 0.40074 0.37667 0.22546 0.36404 0.26994 &
       0.40119 0.40774 0.38113 0.44155 0.45377 0.85824 1.10049 1.75061 &
       1.05885 0.69473 0.95423 1.28806 1.61791 3.42736 5.08625 4.93849 &
       5.76215 6.24544 7.63919 9.09448 10.72170 12.99698 15.11901 17.72156 &
       20.23016 22.56590 26.40307 28.53329 31.99115 35.08662 38.59192 &
       40.72148 44.83722 47.57097 49.83911 52.05385 55.23979 57.19599 &
       58.32202 61.44173 61.60535 63.11445 63.15375 63.94899 64.34468 &
       63.76226 62.89982 61.38343 59.90985 56.63120 55.03628 50.29043 &
       46.85466 41.14607 36.17321 28.71483 21.28540 7.55220 0.29617 0.0000 &
       0.03439 0.00000 0.02957 0.01531 0.00824 0.02051 0.00161 $FLUENCE 16.3
c    2.5 metre Source
c
c Tally cards:
f4:p 1
f6:p 1
c  *f8:p 1
c Tally Energy Ranges:
e4 0 1E-5 10I 0.022 0.025
e6 0 1E-5 10I 0.022 0.025
c  e8 0 1E-5 10I 0.022 0.025
c
c Output:
c print 85 for material data; 161 for bin graphs
print 110 120 130 160 162
c Problem Cutoffs:
phys:p 1 0 0
nps 100000000
```

APPENDIX C

MCNP Input File for Slab Filter Design

The MCNP input file provided below was used to simulate the TLD design that featured a PTFE slab filter. The file corresponds to the device's exposure to the ISO Narrow Series 16 keV source supplied by PTB, incident at zero degrees. Similar files exist for the other energies and angles considered.

```
MCNP input for TLD with PTFE Slab Filter
c Cell cards...
c Card:
    1     1  -2.49      -1 $  Thick LiF
    2     1  -2.49      -2 $  Thin LiF
    3     2  -2.2       1 -3 $ Thick Teflon Cover
    4     2  -2.2       2 -4 $ Thin Teflon Cover
    5     2  -2.2       3 4 -5 -16 $ Teflon Sheet
    6     3  -0.00120484 -6 3 5 $ Air Front Thick
    7     3  -0.00120484 -7 4 5 $ Air Front Thin
    8     3  -0.00120484 -8 5 $ Air Front Right
    9     3  -0.00120484 -9 5 $ Air Front Left
   10     3  -0.00120484 -10 3 5 $ Air Back Thick
   11     3  -0.00120484 -11 4 5 $ Air Back Thin
   12     3  -0.00120484 -12 5 $ Air Back Right
   13     3  -0.00120484 -13 5 $ Air Back Left
   14     4  -2.68      6 7 8 9 -14 -16 $ Aluminium Front
   15     4  -2.68      10 11 12 13 -15 -16 $ Aluminium Back
   16     3  -0.00120484 -5 16 $ Teflon Corner cutoff
   17     3  -0.00120484 -14 16 $ Aluminium Front Corner Cutoff
   18     3  -0.00120484 -15 16 $ Aluminium Back Corner Cutoff
c Wrapper:
   19     5  -0.93      5 14 15 -17 $ EVA Layer
   20     6  -1.39      17 -18 $ PET Layer
c PTFE:
   21    41  -2.2       18 -19 $ PTFE Layer
c Holder:
   22     7  -0.9       18 19 -20 $ Holder back and sides
   23     7  -0.9       -21 $ Holder Front
c Phantom:
   28     8  -1         -28 $ Water Fill
   29     9  -1.19      28 -29 $ Perspex Box
```

```
c Surroundings:
   33     0  20 21 29 -31 $ Vacuum for Kerma Approx.
c Void:
   99     0  31

c Surface cards...
c For the LiF:
    1       rcc    1.28551    -0.7321    -0.3027        0      $ Thick LiF
                0      0.038       0.18
    2       rcc   -1.28551    -0.7321    -0.2962        0      $ Thin LiF
                0      0.025       0.18
c For the Teflon:
    3       rcc    1.28551    -0.7321    -0.3091        0      $ Thick Tef
                0     0.0508     0.1864
    4       rcc   -1.28551    -0.7321    -0.3026        0      $ Thin Tef
                0     0.0378     0.1864
    5       rpp   -2.17551    2.17551    -1.5621     1.5621 $ Teflon Sheet
                 -0.2901     -0.2773
c For the Front Air Cylinders:
    6       rcc    1.28551    -0.7321    -0.3612        0      0 $ Thick F
                   0.0711        0.5
    7       rcc   -1.28551    -0.7321    -0.3612        0      0 $ Thin F
                   0.0711        0.5
    8       rcc    1.28551     0.7321    -0.3612        0      0 $ Right F
                   0.0711        0.5
    9       rcc   -1.28551     0.7321    -0.3612        0      0 $ Left F
                   0.0711        0.5
c For the Back Air Cylinders:
   10       rcc    1.28551    -0.7321    -0.2773        0      0 $ Thick B
                   0.0711        0.5
   11       rcc   -1.28551    -0.7321    -0.2773        0      0 $ Thin B
                   0.0711        0.5
   12       rcc    1.28551     0.7321    -0.2773        0      0 $ Right B
                   0.0711        0.5
   13       rcc   -1.28551     0.7321    -0.2773        0      0 $ Left B
                   0.0711        0.5
c For the Aluminium:
   14       rpp  -2.17551    2.17551    -1.5621     1.5621    $ Front Al
                -0.3612    -0.2901
   15       rpp  -2.17551    2.17551    -1.5621     1.5621    $ Front Al
                -0.2773    -0.2062
c Corner Cut-off Plane:
   16         p          1        -1        0        3.23761
c For the Wrapper:
   17       rpp   -2.17931    2.17931    -1.5659     1.5659    $ EVA layer
                -0.365    -0.2024
   18       rpp   -2.18171    2.18171    -1.5683     1.5683    $ PET layer
                -0.3674   -0.2
```

```
c For the PTFE:
   19       rpp   -2.18171    2.18171    -1.5683     1.5683   $ PTFE layer
                 -0.7374    -0.3674
c For the Holder:
   20       rpp      -2.78      2.78     -2.16      2.16  $ Back and Sides
                 -0.7374     0
   21       rpp      -2.78      2.78     -2.16      2.16   -0.9374 $ Front
                  -0.7374
c For the Phantom:
   28       rpp  -13.60171   14.39829       -14        14     $ Water fill
                 0.25       14
   29       rpp  -14.60171   15.39829       -15        15        0   $ Box
                  15
c For the Surroundings:
   31       rpp  -23.60171   23.39829       -23        23      -26   $ Air
                  15.1
c For the Sources:
   32        pz    -1.1674 $ 0 Degrees (Sources disks centred on 0,0,0)
   33         p          1          0   1.732051      -15.5 $ 30 Degs
   34         p          1          0  0.5773503      -15.5 $ 60 Degs

mode  p
c Materials Specs:
m1    3007.         -0.266167 $ LiF:Mg,Cu,P
      3006.           -8e-005 9000.         -0.728752 12000.        -0.002
      29000.          -4e-005 15000.           -0.003
m2    6000.         -0.240183 $ Teflon
      9000.         -0.759817
m3    6000.         -0.000124 $Air
      7000.         -0.755267 8000.         -0.231781 18000.     -0.012827
m4    14000.          -0.0025 $ Aluminium card
      29000.           -0.001 12000.           -0.025 26000.        -0.004
      25000.           -0.001 24000.          -0.0025 30000.        -0.001
      13000.           -0.963
m41   6000.           0.33333 $ PTFE
      9000.           0.66666
m5    6000.           0.33333 $ EVA
      1000.           0.55556 8000.           0.11111
m6    6000.           0.45455 $ PET
      1000.           0.36364 8000.           0.18182
m7    1000.         -0.143711 $ Polypropylene
      6000.         -0.856289
m8    1000.         -0.111894 $ Water
      8000.         -0.888106
m9    1000.         -0.080538 $ Perspex
      6000.         -0.599848 8000.         -0.319614
c
c Cell Importancies:
```

```
imp:p  128        1          64         1          32         $ 1, 5
       1r         1          11r        32         1r         $ 6, 20
       16         1          16         1          2r         $ 21, 33
       0          $ 99, 99
c
c Source Definition:
sdef POS=0 0 -1.1674 SUR=32 RAD=d1 VEC=0 0 1 DIR=1 PAR=2 ERG=d3 $ ZERO
si1  22
si3  h 0.007 0.0072 0.0074 0.0076 0.0078 0.008 0.0082 0.0084 0.0086 0.0088 &
       0.009 0.0092 0.0094 0.0096 0.0098 0.01 0.0102 0.0104 0.0106 0.0108 &
       0.011 0.0112 0.0114 0.0116 0.0118 0.012 0.0122 0.0124 0.0126 0.0128 &
       0.013 0.0132 0.0134 0.0136 0.0138 0.014 0.0142 0.0144 0.0146 0.0148 &
       0.015 0.0152 0.0154 0.0156 0.0158 0.016 0.0162 0.0164 0.0166 0.0168 &
       0.017 0.0172 0.0174 0.0176 0.0178 0.018 0.0182 0.0184 0.0186 0.0188 &
       0.019 0.0192 0.0194 0.0196 0.0198 0.02 0.0202 0.0204 0.0206 0.0208 &
       0.021 0.0212 0.0214 0.0216 0.0218 0.022  $ ENERGY 16.3
c
sp3  d 0 0.58542 0.23504 0.44782 0.40074 0.37667 0.22546 0.36404 0.26994 &
       0.40119 0.40774 0.38113 0.44155 0.45377 0.85824 1.10049 1.75061 &
       1.05885 0.69473 0.95423 1.28806 1.61791 3.42736 5.08625 4.93849 &
       5.76215 6.24544 7.63919 9.09448 10.72170 12.99698 15.11901 17.72156 &
       20.23016 22.56590 26.40307 28.53329 31.99115 35.08662 38.59192 &
       40.72148 44.83722 47.57097 49.83911 52.05385 55.23979 57.19599 &
       58.32202 61.44173 61.60535 63.11445 63.15375 63.94899 64.34468 &
       63.76226 62.89982 61.38343 59.90985 56.63120 55.03628 50.29043 &
       46.85466 41.14607 36.17321 28.71483 21.28540 7.55220 0.29617 0.0000 &
       0.03439 0.00000 0.02957 0.01531 0.00824 0.02051 0.00161 $FLUENCE 16.3
c    2.5 metre Source
c
c Tally cards:
f4:p 1
f6:p 1
c  *f8:p 1
c Tally Energy Ranges:
e4 0 1E-5 10I 0.022 0.025
e6 0 1E-5 10I 0.022 0.025
c  e8 0 1E-5 10I 0.022 0.025
c
c
c Output:
c print 85 for material data; 161 for bin graphs
print 110 120 130 160 162
c Problem Cutoffs:
phys:p 1 0 0
nps 100000000
```

APPENDIX D

MCNP Input File for Final Design

The configuration shown below represents the MCNP input corresponding to the final design of the new HPA TLD, which features a holder incorporating an 18 mm diameter, 4.3 mm thick PTFE disk filter covered by 2 mm of PP. As in Appendices B and C, the file provided relates to exposure to the 16 keV ISO Narrow Series source supplied by PTB incident at zero degrees, but similar inputs exist for the other energies and angles that were of interest.

```
MCNP input for Final TLD Holder Design
c Cell cards...
c Card:
    1     1  -2.49      -1 $  Thick LiF
    2     1  -2.49      -2 $  Thin LiF
    3     2  -2.2       1 -3 $ Thick Teflon Cover
    4     2  -2.2       2 -4 $ Thin Teflon Cover
    5     2  -2.2       3 4 -5 -16 $ Teflon Sheet
    6     3  -0.00120484 -6 3 5 $ Air Front Thick
    7     3  -0.00120484 -7 4 5 $ Air Front Thin
    8     3  -0.00120484 -8 5 $ Air Front Right
    9     3  -0.00120484 -9 5 $ Air Front Left
   10     3  -0.00120484 -10 3 5 $ Air Back Thick
   11     3  -0.00120484 -11 4 5 $ Air Back Thin
   12     3  -0.00120484 -12 5 $ Air Back Right
   13     3  -0.00120484 -13 5 $ Air Back Left
   14     4  -2.68      6 7 8 9 -14 -16 $ Aluminium Front
   15     4  -2.68      10 11 12 13 -15 -16 $ Aluminium Back
   16     3  -0.00120484 -5 16  $ Teflon Corner cutoff
   17     3  -0.00120484 -14 16 $ Aluminium Front Corner Cutoff
   18     3  -0.00120484 -15 16 $ Aluminium Back Corner Cutoff
c Wrapper:
   19     5  -0.93      5 14 15 -17 $ EVA Layer
   20     6  -1.39      17 -18 $ PET Layer
   21     3  -0.00120484 18 -19 $ Air Jacket
c Holder:
   22     7  -0.9       19 -20 $ Holder back and sides
   23    41  -2.2       -21 $ PTFE disk
   24     7  -0.9       21 24 -23 25 $ Front Face
   25     3  -0.00120484 21 -24 $ Air Window
```

```
   26     3  -0.00120484 -23 -25 $ Cone Cutout
   27     7  -0.9       21 -26 $ Cylindrical Front Lump
c Phantom:
   28     0  -28 $ Water Fill
   29     0  28 -29 $ Perspex Box
c Environment:
   30     0  20 23 26 29 -31 $ Air or Vacuum for Kerma Approx.
c  Void:
   99     0  31

c Surface cards...
c For the LiF:
    1       rcc    1.28551    -0.7321    -0.3027        0      $ Thick LiF
                 0      0.038       0.18
    2       rcc   -1.28551    -0.7321    -0.2962        0      $ Thin LiF
                 0      0.025       0.18
c For the Teflon:
    3       rcc    1.28551    -0.7321    -0.3091        0      $ Thick Tef
                 0     0.0508     0.1864
    4       rcc   -1.28551    -0.7321    -0.3026        0      $ Thin Tef
                 0     0.0378     0.1864
    5       rpp   -2.17551    2.17551    -1.5621     1.5621 $ Teflon Sheet
                  -0.2901     -0.2773
c For the Front Air Cylinders:
    6       rcc    1.28551    -0.7321    -0.3612        0      0 $ Thick F
                    0.0711        0.5
    7       rcc   -1.28551    -0.7321    -0.3612        0      0 $ Thin F
                    0.0711        0.5
    8       rcc    1.28551     0.7321    -0.3612        0      0 $ Right F
                    0.0711        0.5
    9       rcc   -1.28551     0.7321    -0.3612        0      0 $ Left F
                    0.0711        0.5
c For the Back Air Cylinders:
   10       rcc    1.28551    -0.7321    -0.2773        0      0 $ Thick B
                    0.0711        0.5
   11       rcc   -1.28551    -0.7321    -0.2773        0      0 $ Thin B
                    0.0711        0.5
   12       rcc    1.28551     0.7321    -0.2773        0      0 $ Right B
                    0.0711        0.5
   13       rcc   -1.28551     0.7321    -0.2773        0      0 $ Left B
                    0.0711        0.5
c For the Aluminium:
   14       rpp   -2.17551    2.17551    -1.5621     1.5621    $ Front Al
                 -0.3612    -0.2901
   15       rpp   -2.17551    2.17551    -1.5621     1.5621    $ Front Al
                 -0.2773    -0.2062
c Corner Cut-off Plane:
   16         p          1         -1          0    3.23761
```

```
c For the Wrapper:
   17       rpp   -2.17931    2.17931    -1.5659     1.5659    $ EVA layer
                 -0.365    -0.2024
   18       rpp   -2.18171    2.18171    -1.5683     1.5683    $ PET layer
                 -0.3674   -0.2
c For the Air Gaps:
   19       rpp       -2.9       2.9     -1.75      1.75    $ Air Jacket
                 -0.3674   -0.2
c For the Holder:
   20       rpp       -3.1       3.1     -1.95      1.95  $ Back and Sides
                 -0.3674    0
c For the Filter:
   21       rcc    1.28551    -0.7321    -0.7974       0     0 $ PTFE disk
                  0.43      0.9
c For the Front Face:
   23       rpp       -3.1       3.1      -1.95       1.95 $ Plastic front
                 -0.5674    -0.3674
   24       rpp      -2.25       2.25      0.42       1.62 $ Air Window
                 -0.5674    -0.3674
   25       k/z   -1.28551    -0.7321     0.4326     0.5625  -1    $ Cone
   26       rcc    1.28551    -0.7321    -0.9974          0   0    $ Lump
                  0.43      1.1
c For the Phantom:
   28       rpp  -13.60171   14.39829      -14        14      $ Water fill
                 0.25       14
   29       rpp  -14.60171   15.39829      -15        15      0     $ Box
                    15
c For the Surroundings:
   31       rpp        -35         35      -23        23      -26   $ Air
                    35
c For the Source:
   32        pz    -1.1674 $ 0 Degrees (Source disks centred on 0,0,0)
   33         p          1          0   11.43005       15.5 $ 5 Degrees
   34         p          1          0   5.671282       15.5 $ 10 Degrees
   35         p          1          0   3.732051       15.5 $ 15 Degrees
   36         p          1          0   2.747477       15.5 $ 20 Degrees
   37         p          1          0   2.144507       15.5 $ 25 Degrees
   38         p          1          0   1.732051       15.5 $ 30 Degrees
   39         p          1          0   1.428148       15.5 $ 35 Degrees
   40         p          1          0   1.191754       15.5 $ 40 Degrees
   41         p          1          0          1       15.5 $ 45 Degrees
   42         p          1          0  0.7002075       15.5 $ 50 Degrees
   43         p          1          0  0.5773503       15.5 $ 55 Degrees
   44         p          1          0  0.5773503       15.5 $ 60 Degrees
   45         p          1          0  0.4663077       15.5 $ 65 Degrees
   46         p          1          0  0.3639702       15.5 $ 70 Degrees
   47         p          1          0  0.2679492       15.5 $ 75 Degrees
   48         p          1          0   0.176327       15.5 $ 80 Degrees
```

```
   49         p          1          0 0.08748866       15.5 $ 85 Degrees
   50         p          1          0          0       15.5 $ 90 Degrees
   51         p          1          0 -0.08748866      15.5 $ 95 Degrees
   52         p          1          0  -0.176327       15.5 $ 100 Degrees
   53         p          1          0 -0.2679492       15.5 $ 105 Degrees
   54         p          1          0 -0.3639702       15.5 $ 110 Degrees
   55         p          1          0 -0.4663077       15.5 $ 115 Degrees
   56         p          1          0 -0.5773503       15.5 $ 120 Degrees

mode  p
c Materials Specs:
m1    3007.         -0.266167 $ LiF:Mg,Cu,P
      3006.           -8e-005 9000.         -0.728752 12000.        -0.002
      29000.          -4e-005 15000.           -0.003
m2    6000.         -0.240183 $ Teflon
      9000.         -0.759817
m3    6000.         -0.000124 $Air
      7000.         -0.755267 8000.         -0.231781 18000.     -0.012827
m4    14000.          -0.0025 $ Aluminium card
      29000.           -0.001 12000.           -0.025 26000.        -0.004
      25000.           -0.001 24000.          -0.0025 30000.        -0.001
      13000.           -0.963
m41   6000.            0.3333 $ PTFE
      9000.            0.6666
m5    6000.           0.33333 $ EVA
      1000.           0.55556 8000.           0.11111
m6    6000.           0.45455 $ PET
      1000.           0.36364 8000.           0.18182
m7    1000.         -0.143711 $ Polypropylene
      6000.         -0.856289
m8    1000.         -0.111894 $ Water
      8000.         -0.888106
m9    1000.         -0.080538 $ Perspex
      6000.         -0.599848 8000.         -0.319614
c
c Cell Importancies:
imp:p  128         1r          64          1r          16          $ 1, 5
       32          12r         16          5r          1           $ 6, 25
       16          1r          1           2r          0          $ 26, 99
c
c Source Definition:
sdef POS=0 0 -1.1674 SUR=32 RAD=d1 VEC=0 0 1 DIR=1 PAR=2 ERG=d3 $ ZERO
si1  22
si3  h 0.007 0.0072 0.0074 0.0076 0.0078 0.008 0.0082 0.0084 0.0086 0.0088 &
       0.009 0.0092 0.0094 0.0096 0.0098 0.01 0.0102 0.0104 0.0106 0.0108 &
       0.011 0.0112 0.0114 0.0116 0.0118 0.012 0.0122 0.0124 0.0126 0.0128 &
       0.013 0.0132 0.0134 0.0136 0.0138 0.014 0.0142 0.0144 0.0146 0.0148 &
       0.015 0.0152 0.0154 0.0156 0.0158 0.016 0.0162 0.0164 0.0166 0.0168 &
```

```
       0.017 0.0172 0.0174 0.0176 0.0178 0.018 0.0182 0.0184 0.0186 0.0188 &
       0.019 0.0192 0.0194 0.0196 0.0198 0.02 0.0202 0.0204 0.0206 0.0208 &
       0.021 0.0212 0.0214 0.0216 0.0218 0.022  $ ENERGY 16.3
c
sp3  d 0 0.58542 0.23504 0.44782 0.40074 0.37667 0.22546 0.36404 0.26994 &
       0.40119 0.40774 0.38113 0.44155 0.45377 0.85824 1.10049 1.75061 &
       1.05885 0.69473 0.95423 1.28806 1.61791 3.42736 5.08625 4.93849 &
       5.76215 6.24544 7.63919 9.09448 10.72170 12.99698 15.11901 17.72156 &
       20.23016 22.56590 26.40307 28.53329 31.99115 35.08662 38.59192 &
       40.72148 44.83722 47.57097 49.83911 52.05385 55.23979 57.19599 &
       58.32202 61.44173 61.60535 63.11445 63.15375 63.94899 64.34468 &
       63.76226 62.89982 61.38343 59.90985 56.63120 55.03628 50.29043 &
       46.85466 41.14607 36.17321 28.71483 21.28540 7.55220 0.29617 0.0000 &
       0.03439 0.00000 0.02957 0.01531 0.00824 0.02051 0.00161 $FLUENCE 16.3
c    2.5 metre Source
c
c Tally cards:
f4:p 1 2
f6:p 1 2
c   *f8:p 1
c Tally Energy Ranges:
e4 0 1E-5 10I 0.022 0.025
e6 0 1E-5 10I 0.022 0.025
c   e8 0 1E-5 10I 0.022 0.025
c
c Output:
c print 85 for material data; 161 for bin graphs
print 110 120 130 160 162
c Problem Cutoffs:
phys:p 1 0 0
nps 100000000
```